NOAA Technical Memorandum ERL ARL-201

INVESTIGATION OF ATMOSPHERIC AEROSOLS AND GASES AT AN EAST CHINA STATION

Farn Parungo
Clarence Nagamoto
Barbara Kopcewicz
Xingsheng Li
Dongzeng Yang
Xiaolan Yu
Joyce Harris

Air Resources Laboratory
Silver Spring, Maryland
April 1993

noaa NATIONAL OCEANIC AND ATMOSPHERIC ADMINISTRATION / Environmental Research Laboratories

NOAA Technical Memorandum ERL ARL-201

INVESTIGATION OF ATMOSPHERIC AEROSOLS AND GASES AT AN EAST CHINA STATION

Farn Parungo
Clarence Nagamoto
Barbara Kopcewicz
Aerosol Research Section
Air Resources Laboratory
Boulder, Colorado

Xingsheng Li
Dongzeng Yang
Xiaolan Yu
Academy of Meteorological Science
Beijing, China

Joyce Harris
Climate Monitoring and Diagnostics Laboratory
Boulder, Colorado

Air Resources Laboratory
Silver Spring, Maryland
April 1993

UNITED STATES
DEPARTMENT OF COMMERCE

NATIONAL OCEANIC AND
ATMOSPHERIC ADMINISTRATION

Environmental Research
Laboratories

NOTICE

Mention of a commercial company or product does not constitute an endorsement by the NOAA Environmental Research Laboratories. Use of information from this publication concerning proprietary products or the tests of such products for publicity or advertising purposes is not authorized.

For sale by the National Technical Information Service, 5285 Port Royal Road
Springfield, VA 22061

CONTENTS

TABLES

FIGURES

Investigation of Atmospheric Aerosols and Gases at an East China Station

F. Parungo, C. Nagamoto, B. Kopcewicz, X. Li, D. Yang, X Yu, and J. Harris

ABSTRACT. From August to October of 1991, when the West Pacific Exploratory Mission (PEM-west) airborne expedition was conducted, ground-level measurements of gases and aerosols were carried out at Lin-an station near the east coast of China. Meteorological parameters such as temperature, pressure, humidity, solar radiation, wind direction, and wind speed were recorded continuously. Concentrations of SO_2, NO_2, O_3, and black carbon were monitored in situ intermittently. Aerosol samples were collected and later analyzed in laboratories. A transmission electron microscope was used to analyze particle concentration, morphology, and size distribution. Elemental compositions of aerosol samples, collected on filters, were determined with an neutron activation analyzer and with a proton induced x-ray energy spectrometer. The water soluble portions of the aerosols were analyzed by ion chromatography. All measurements were recorded in the PEM-west archive. The averages, or the medians, of all measured quantities as well as their standard variations or confidence intervals are documented in this report. The results show that the concentrations of both natural crustal dust and anthropogenic air pollution were very high at this rural station. Most crustal elements (e.g., Al, Si, Fe, Sc) were present in larger particles ($d > 1\ \mu m$), whereas most enriched elements (e.g., S, As, Sb) were in smaller particles. Concentrations of sea-salt ions Na^+, Mg^{++}, and Cl^- were not high, and they were found in large particles. Concentrations of $SO_4^=$ and NH_4^+ correlated well with each other ($r=0.81$), and they were found mostly in small particles. Concentrations of NO_3^-, which were < one-fifth of the concentrations of $SO_4^=$, also correlated significantly with $SO_4^=$ ($r=0.79$). Most NO_3^- mass was present in large particles. The variability of air chemistry is mostly influenced by local wind direction and wind speed as well as long-distance air trajectories. Solar radiation also played a role in SO_2-gas-to-$SO_4^=$-particle conversion. Rainfall appeared to be an effective way to wash out air contaminants and to improve air quality. However, the effect was generally short-lived. The result of this investigation provided a basic understanding of trace species in the regional surface air, including their sources, transport, transformations, and sinks. The data sets collected at the station can be used as a source inventory for long-range transport of air masses from China to the West Pacific Ocean. Such journeys are believed to have a profound impact on climatic changes.

1. INTRODUCTION

Inadvertent weather modification and climate changes, affected by anthropogenic air pollution, have caused increasing concerns. For example, greenhouse gases such as carbon dioxide, methane, and water vapor whose concentrations increase with human activities, are considered to be culprits in global warming; florochlorocarbons, which have been widely used in industrial nations, may deplete stratospheric ozone; and sulfate aerosols, which are active cloud condensation nuclei, have the potential of modifying cloud characteristics and thus changing cloud lifetimes, the radiation budget, or precipitation amounts. Because of these critical problems facing the global environment, it is important to understand the life cycles of each affecting species in the air. Knowing the strengths of the pollution sources, the transport and the distribution of the plumes, the interactions among the species, and their rates of wet and dry deposition, one can analyze quantitatively their impacts on the atmosphere. Therefore, measurements of atmospheric trace species are essential to verify any sophisticated models for the purpose of accurately predicting climatic changes such as a trend, a pattern, or the rate of change. Unfortunately, we lack comprehensive databases for many atmospheric trace species at this time. The inadequacy is especially profound in many populated developing nations, where the pollution sources have been very strong, but the air pollution controls remain weak.

It was the purpose of this investigation to obtain data sets of several major air pollutants at Lin-an station in eastern China. The research is a part of a multinational program, called the Pacific Exploratory Mission-west (PEM-west), led by the scientists from the National Oceanic and Atmospheric Administration (NOAA) and National Aeronautics and Space Administration (NASA). Many scientists from the United States, China, Korea, Japan, Taiwan, and Hong Kong have collaborated in this program. The overall mission was to explore the tropospheric chemistry over the Western Pacific Ocean. Both airborne and surface measurements were conducted in the autumn of 1991 (Liu, 1992). Our project was to investigate the source strength of air pollution from China.

Lin-an station (119° 44'E, 30° 48'N, and 140 m MSL), situated on a rural mountain near the central east coast of China (see Fig. 1), 200 km southwest of Shanghai city (population 13 million), 40 km west-northwest of Hangzhou city (population 5.8 million), and 12 km northeast of Lin-an city (population 0.5 million). The region is renowned as a food basket of China, with lavish rice fields and farm lands. Both heavy and light industries are plentiful, and air pollution has been presenting a serious problem. The station was selected to avoid contamination of local point sources. and the measurements at the station should represent the regional background air chemistry. The measurements provide a database of regional air quality, which is needed for the PEM-west program for the source strengths for long-range transport. This paper reports our measurements and the analyses of atmospheric aerosols and gases. The transport and transformation of several specific species are also discussed.

2. MEASUREMENTS AND ANALYSES

From August to October 1991 air chemistry measurements were conducted at Lin-an station, at the same time that airborne measurements were carried out by NASA and NOAA scientists over the Western Pacific with a DC-8 aircraft. At the station, SO_2, NO_2, O_3, and black carbon were measured intermittently in real time, and wind speed, wind direction, and solar radiation were measured continuously. Aerosol samples were collected on filters and on microgrids for laboratory analyses.

The instrument used for SO_2 measurement is a modified fluorescence analyzer (TEI model 43s, Thermo-Environmental Inc.). Its precision is better than 0.1 ppbv with a minimum detection limit of 0.05 ppbv. The response time is 10 seconds, and data outputs were averaged every minute. The detailed procedures for calibration and operation were reported by Luria et al. (1992). Concentration of O_3 was determined with a fluorescence analyzer. A chemiluminescence analyzer for NO and NO_2 (Thermo-Environmental Inc.) was operated by scientists from Georgia Institute of Technology (M. Rodgers, private communication). Their NO_2 concentration data were available to us for comparisons.

An automatic aethalometer (Magee Scientific Co.; Hansen and Novakov, 1988) was used to measure black carbon. It measures optical absorption of aerosols collected on a quartz filter. The minimum detection limit is 1 ng m^{-3}, and the data output is regulated to every minute.

Temperature, pressure, humidity, solar radiation, wind direction, and wind speed were automatically recorded at the station. All the real-time measurements were acquired simultaneously with a computer and archived into a data system.

Atmospheric aerosols were collected using three methods for different analytical purposes: (1) A one-stage sampler (KB-120, made in China) was used to collect particles on Teflon filters (90 cm diameter, 1 μm pore, with collection efficiency > 99.9% for particle diameter d > 0.1 μm). The sampling flow rate was regulated to 110 L min^{-1}, and the sampling time ranged from 6 to 10 hours. Generally, one sample was collected during the day and one at night. The samples were used for bulk chemical analyses. (2) An eight-stage Anderson sampler was used to segregate particles according to their aerodynamic sizes on Teflon filters. The sampling flow rate was 28.3 L min^{-1}, and sampling time was planned for 2 days, but actual sampling periods varied from 15 to 46 hours because of rain or other interruptions. These samples were used to determine mass distributions with respect to particle size for various elements and ions. (3) A four-stage cascade impactor (Cassella) was used to collected particles on electron-microscope grids that were covered with Formvar film and coated with carbon. The flow rate was 17.5 L min^{-1}, and the sampling time was 30 minutes. The samples were analyzed with a transmission electron microscope (TEM) for individual particle morphology and aerosol number size distribution. Using a chemical spot test, one can also identify individual particles containing sulfate with a TEM. Detailed analytical procedures were reported by Bigg et al. (1974) and Parungo et al. (1986).

The Teflon filter samples were bisectioned. One set of halves was sent to the Institute of High Energy Physics, Chinese Academy of Science, Beijing, where neutron activation analysis (NAA) and proton induced x-ray energy (PIXE) spectrometry were used to determine the concentrations of trace elements in the aerosol samples. The analytical procedures and their accuracies were discussed by Zhou et al. (1990). The other set of halves was analyzed at the NOAA Air Resources Laboratory at Boulder, Colorado, U.S.A., with an ion chromatograph (IC) to determine ion concentrations of water soluble portions of the aerosols.

3. MEASUREMENT RESULTS AND DATA REDUCTION

3.1. SO_2 Concentrations

The concentrations of gases fluctuated with wind direction. Figure 2 shows the distributions of hourly averages of SO_2 concentrations in eight wind sectors (SO_2 "rose"). The concentrations ranged from 0.1 to 35 ppbv. The maximum concentration occurred when the prevailing winds were from the northeast, where Shanghai is located, and the minimum was observed during southeasterlies from the sea. Although the station is at a secluded site, the median SO_2 concentrations in all wind sectors were 2-7 ppbv, which were very high compared with NOAA/Climate Monitoring and Diagnostics Laboratory (CMDL) baseline stations, which had mean concentrations <0.1 ppbv. However, it is comparable with annual mean SO_2 concentrations (4-6 ppb) at the eastern seaboard stations of the United States (NAPAP, 1987).

The SO_2 concentration varied also with solar radiation. Figure 3 demonstrates its diurnal variation from 20 to 24 August, which were cloudless, sunny days. In the first 3 days, the SO_2 concentrations at night were as high as 20 ppbv. After sunrise, the concentrations began to decrease and reached minima (<2 ppbv) in the afternoon, then increased again after sunset. This indicated that SO_2 could be oxidized to form sulfate particles more rapidly in the daytime than at night. The high SO_2 concentrations at nighttime could also be attributed by the stable nocturnal boundary layer, which capped local pollution from convection. On 24 August the wind direction changed to northwesterly. The SO_2 concentrations decreased below 5 ppbv for most the day, and no diurnal variation was observed. Additional SO_2 measurements (Figs. 4-6) show that diurnal variations were not always observed. Other meteorological parameters perhaps play a dominant role on those occasions.

3.2. NO_2 Concentrations

The concentrations of NO_2, which were also strongly influence by wind direction, showed fluctuations similar to the SO_2 concentrations, suggesting their common sources and pathways. On 21-23 August the NO_2 diurnal variations observed were like those of SO_2, with maxima at night (6 ppbv) and minima (3 ppbv) in the afternoon (Fig. 3). This implies that NO_2 gas was probably being converted to nitrate particles during the day by photo-oxidation. However, the NO_2 diminishing rate in the morning was not as fast as that of SO_2.

3.3. O_3 Concentrations

Unlike SO_2 and NO_2 concentrations, O_3 concentrations had an opposite diurnal variation, with a maximum (90 ppbv) in the afternoon and a minimum (20 ppbv) before sunrise (Figs. 3-6). This diurnal variation probably reflects photo-production of O_3, as expected.

3.4. Black Carbon Concentrations

The real-time measurements of black carbon (BC) also showed a great variability. Figure 7 shows the distributions of BC hourly average concentrations in eight wind directions (BC rose). The widest variation and the highest median concentration (2.7 $\mu g\ m^{-3}$) were observed during northeast winds, which probably had transported some air pollution from Shanghai. Nearby Lin-an city was also a strong source, delivering BC from the southwest with a median concentration of 2.0 $\mu g\ m^{-3}$. Even when the winds were from the eastern ocean or the western mountains, the median BC concentrations were still between 1 and 2 $\mu g\ m^{-3}$. The high BC concentrations measured at the station probably reflect the high consumption rate of coal in China (1×10^9 tons in 1987 and still increasing). Coal is the major fuel for industrial and domestic energy (Wang and Shi, 1991). In addition, agriculture biomass burning in the region may also contribute to the high BC concentrations in the air.

Unlike the concentrations of gases, BC aerosols did not show a discernible diurnal variation. This is probably due to the facts (a) that BC is chemically inert to solar radiation, and thus its concentration is not affected by the photo-oscillation of day and night, (b) that although higher concentrations may be expected at night because of the lower planetary boundary layer (PBL), BC production is lower at night because of reduced activities, and (c) that large carbon particles have greater dry deposition velocity than gases, and thus the larger sized portions may reside in the air for too short a time to exhibit a predictable variation.

3.5. Aerosol Mass Concentrations

To reach the sensitivity of NAA, PIXE, or IC for bulk chemical analyses, large volumes of air must be pumped through the filters for several hours. Thus, the temporal resolutions for aerosol concentrations were crude. The samples were classified into only two classes, day and night. During such long periods atmospheric conditions (i.e., wind direction) often had changed. And thus, it is difficult to correlate aerosol characteristics with wind direction, wind speed, or other meteorological parameters.

The Teflon filters were dried in a desiccator and weighed individually prior to use. Among 51 samples collected with the KB-120 sampler, 27 samples were collected during the day and, 24 were collected at night. The sampled filters were dried and weighed again to obtain the mass of total suspended particles (TSP). The average TSP concentration was 234 $\mu g\ m^{-3}$ (standard deviation SD = 42.86) for daytime samples and 248.81 $\mu g\ m^{-3}$ (SD = 43.32) for nighttime samples. The difference is not statistically significant at the 95% confidence level. The fact that daytime human activities should produce more

aerosols probably offset the fact that the lower PBL at night can cause higher aerosol concentrations at the surface.

3.6. Elemental Concentrations in Aerosols

Fifty-one aerosol samples were analyzed with NAA for their elemental concentrations. Na, K, Sc, Cr, Fe, Co, Ni, Zn, Ga, As, Se, Br, Rb, Zr, Mo, Ag, Sb, Cs, Ba, La, Ce, Nd, Sm, Eu, Tb, Yb, Lu, Hf, Ta, W, Au, Th, and U were determined through a long irradiation procedure (neutron flux of 6×10^{13} n cm^{-2} s^{-1} for 16-24 h), while Mg, Al, Cl, Ca, Ti, V, Mn, Cu, In, and I were determined through a short irradiation procedure (neutron flux of 8×10^{11} n cm^{-2} s^{-1} for 5 min). Elements Si, S, and Pb, which could not be determined with NAA, were analyzed with PIXE. Table 1 shows the average concentrations of elements X and the average enrichment factor (EF) of X in comparison with the earths crust, using Fe as a reference.

$$EF = [(X/Fe)\text{in aerosol}]/[(X/Fe)\text{ in crust}].$$

The 95% confidence intervals of the mean for each parameter are also listed in Table 1.

Among all the elements analyzed, the concentrations were S > Si > Ca > Al > K > Fe > Na > Mg > Cl > Pb > Ti > Zn, etc. The result indicates that sulfur pollutants and crustal dust are major components in the regional aerosols. Sea-salt particles are minor components. Because neither NAA nor PIXE can analyze common elements H, C, N, and O, the sum of mass concentrations of the elements analyzed accounted for less than one-fifth of the mass of TSP weighed in the same samples.

Elements Pb and S were the most enriched in the aerosols (EF > 10^4 and 10^3 respectively). Elements I, Br. Cl, Sb, Se, Cr, Ag, and Ga also were substantially enriched (EF > 10^2). Elements Zn, As, Mo, In, Cs, W, and Au were moderately enriched (EF ≥ 10). The excess amounts, compared with Fe, were most likely anthropogenic. Gasoline and coal combustion in addition to industrial exhaust probably enhance their concentrations in the aerosols.

3.7. Ion Concentrations in Aerosols

The other halves of the filter samples were extracted with water and analyzed with IC to determine the concentrations of common anions ($SO_4^=$, NO_3^-, Cl^-) and cations (NH_4^+, Na^+, K^+, Ca^{++}, Mg^{++}). Since not all compounds containing Cl, K, Ca, or Mg in aerosols are soluble in water, their ion concentrations, determined with IC, were generally lower than the results of NAA or PIXE analysis. Table 2 lists the average concentrations of the ions analyzed and 95% confidence interval of the mean. The results showed concentrations $SO_4^=$ > NH_4^+ > Ca^{++} > K^+ > NO_3^- > Na^+ > Cl^- > Mg^{++}. Because many ions such as carbonate and organic ions were not determined, the sum of anion equivalences could not balance the sum of cations equivalences.

From IC analysis of filter samples, the average $SO_4^=$ concentration was 14.57 $\mu g\ m^{-3}$ (SD = 6.60) for daytime samples (n = 27), and 15.60 $\mu g\ m^{-3}$ (SD = 7.84) for nighttime samples (n = 24). The difference between day and night for

$SO_4^=$ concentrations was not statistically significant. Because the filter samples, which were collected for as long as 10 hours, generally could not yield a good temporal resolution, the importance of sulfate production by photochemical oxidation of SO_2, followed by homogeneous nucleation, is difficult to assess with this method.

Likewise, photo-oxidation of NO_2 gases should produce more nitrate aerosols in the day than at night. Our measurements showed average concentrations of NO_3^- in aerosols was 1.81 $\mu g\ m^{-3}$ (SD = 2.08) for daytime samples, and 1.78 $\mu g\ m^{-3}$ (SD = 2.12) for nighttime samples. Again the difference between day and night was not significant.

3.8. Aerosol Size Distributions

Filter samples collected with an eight-stage Anderson sampler were weighed and analyzed with NAA, PIXE, and IC. Seven sets of samples were analyzed. The mass fractions of each element at each stage were computed. The size distributions of elements Al, Fe, Co, Sc, and Si are shown in Fig. 8. All these elements had a mass maximum on stage 3 (3.3-4.7 μm). More than 80% of the masses were in supermicron particles, collected on the first six stages, and < 20% were in submicrometer particles, collected on the last two stages. The majority of these particles were probably crust dust. The size distribution of TSP is also shown in Figure 8; the mass was rather evenly distributed on all stages.

Figure 9 shows the size distributions of elements S, As, and Sb. All had a maximum mass in the smallest particles, collected on stage 8 (< 0.43 μm), and > 60% of the masses were in submicrometer particles. These small particles were probably formed through high-temperature combustion followed by gas-to-particle conversion.

Figure 10 shows the size distributions of the ions $SO_4^=$, NO_3^-, Cl^-, NH_4^+, Na^+, K^+, Mg^{++}, and Na^+. Like for the element S, the mass of $SO_4^=$ had a maximum on the last stage (< 0.43 μm), and >80% of the mass was distributed in small particles (< 1.1 μm). Unlike $SO_4^=$, almost all the NO_3^- mass was were present in large particles (> 2.1 μm) with a maximum on stage 3 (3.3-4.7 μm). The mass of Cl^- was accumulated on the first three stages, and very little was in particles smaller than 4.7 μm. The distinctions of size distributions among $SO_4^=$, NO_3^-, and Cl^- suggest diverse sources and mechanisms of formation. Perhaps Cl^- was present in sea-salt or soil particles, which are usually large. Most of the $SO_4^=$ was probably formed through photochemical oxidation of SO_2 to H_2SO_4, which reacted with atmospheric NH_3 to produce $(NH_4)_2SO_4$ or NH_4HSO_4 by homogeneous nucleation. These processes generally produce small particles. In addition, a small portion of SO_2 and H_2SO_4 gases converted to $SO_4^=$ particles through heterogeneous nucleation, which produced a coating over the existing larger particles. The majority of NO_3^- particles were probably formed through photo-oxidation of NO_2 to HNO_3 gas, followed by heterogeneous nucleation and titration on existing particles, and thus the size distribution of NO_3^- particles resembles those crustal elements such as Si, Al, and Sc. Small particles of NH_4NO_3, produced by homogeneous nucleation, are known to be unstable, and can decompose to HNO_3 and NH_3 gases in a dry atmosphere. When the relative humidity is > 62%, which is the NH_4NO_3 deliquescence point, NH_4NO_3

may be present in droplets without decomposition.

The size distribution of NH_4^+ is similar to $SO_4^=$, except only 2% of the NH_4^+ mass was in large particles ($d > 2.1$ μm), while 20% of $SO_4^=$ was in large particles. The data suggest that in small particles $SO_4^=$ combined with $NH4^+$, but in larger particles $SO_4^=$ probably combined with other cations.

The size distribution of K^+ is also skewed toward small particles, which is different from other soil elements. Regional biomass burning, which had occurred quite often, could have produced many small K-containing particles.

Size distributions of Na^+, Mg^{++}, and Ca^{++} showed some similarity, all having a maximum mass on stage 3 (3.3-4.7 μm). These distributions also resembled those of elements Al, Fe, Sc, and Si (Fig. 8). Large soil and sea-salt particles in the samples probably consisted of these elements.

3.9. Morphology of Individual Particles

Aerosol samples collected on electron-microscope grids with the four stage cascade impactor were examined with an transmission electron microscope (TEM) for the morphology of individual particles. Figure 11 depicts the images of particles. Most particles on stage 1 ($d > 5$ μm) were either giant solid dust or loosely conglomerated soot as shown in Fig. 11a. Most particles on stage 2 (2-5 μm) and stage 3 (0.7-2 μm) were irregular shaped (Figs. 11b and 11c). And most small particles on stage 4 ($d < 0.7$ μm) were spheroids (Fig. 11d).

When aerosols were collected on $BaCl_2$-coated grids, particles containing $SO_4^=$ reacted with the coating and formed a hollow ring as shown in Fig. 12. The bigger the ring, the more the $SO_4^=$ a particle contained. The relative thickness (RT) of the ring is defined as the ratio between the thickness of the ring and the radius of the total reaction spot. This test of the RT has been used in our laboratory routinely (Kopcewicz et al., 1991). Of the giant particles on stage 1, (40 ± 30)% contained $SO_4^=$ and the average RT was 0.25 (SD = 0.2). Some consisted of a group of particles at the center (see Fig. 12a), suggesting that conglomeration through liquid-phase interactions probably had taken place. About (60 ± 20) % of the large particles on stages 2 and 3 contained $SO_4^=$ and the average RT 0.5 (SD = 0.1). Inhomogeneous and irregular-shaped centers were generally observed (see Fig. 12b and 12c). This suggests that $SO_4^=$ had formed a coating on the existing particles, probably through heterogeneous nucleation. Approximately (90 ± 10)% of the small particles on stage 4 contained $SO_4^=$, which had rings with RT = 0.75 (SD = 0.05), suggesting they consisted of mostly $SO_4^=$ (see Fig. 12d).

4. DISCUSSION

The measured concentrations of gases and elements/ions in aerosol particles provide general inventories of each species present in the air at the station during the sampling period. Because meteorological conditions vary from season to season, and year to year, the data sets should not be considered as fixed representatives. More measurements are needed in order to reach long-term significant statistics.

The average concentration of total aerosols for 51 samples was 242.1 μg m^{-3} (SD = 43.1), indicating a very dusty and highly polluted environment. The average Al concentration was 4.5 μg m^{-3} (SD = 2.2). According to Taylor and Mclennan (1985) mineral dust that is produced through the weathering of crustal rock and windborne soil dust typically contain approximately 8% Al by weight. Therefore, the average crustal dust concentration was 56.3 μg m^{-3}, which was 23.3% of the total weight of aerosol particles. Crustal elements such as Ba, Ca, Co, Ce, Eu, Fe, Hf, K, La, Lu, Mn. Nd, Ni, Rb, Si, Sc, Sm Ta, Tb, Th, V, and U had EFs generally < 5.

Common sea-salt elements such as Na, Cl, Mg, Br, and I had a wide range of EFs in reference to Fe, and individual EFs did not correlate to one another. This suggests that their sources might not be limited to sea salt. Although Lin-an is < 100 km from the sea coast, the maximum EF for Na^+ was 3. This indicates that sea-salt particles were not a major contributor to the regional total aerosols.

Elements with the highest EFs were most likely from anthropogenic air pollution: Pb, S, Sb, Se, Cr, Ag, As, Zn, Mo, and W had EFs ranging from one to four orders of magnitude (see Table 1). In general the concentrations of these enriched elements were poorly correlated with one another, indicating their diverse origins. Perhaps Pb was from gasoline combustion, S, Se, and Sb were from coal fire; and As, Ag, Zn, Mo and other elements were from ore smelting. Most of these elements were present in small particles, probably being produced by vaporization at high temperature, followed by gas-to-particle conversion.

Among anthropogenic aerosols, sulfate, nitrate, and ammonium particles had precursor gases, SO_2, NO_x, and NH_3, respectively. To understand the measurement results, one must analyze the fluctuations of atmospheric conditions during the sampling periods. In addition to the meteorological measurements at the station, two long-range air trajectory maps for each day (0000 and 1200 UT) were computed using the NOAA/CMDL isobaric model for 10-day backward air mass pathways at 500, 700, 850, and 1000 hPa levels (Harris, 1982). The information is very useful in interpreting the chemistry of air masses that arrived at the station.

20-23 August the air trajectory at 500 hPa was westerly, but at lower levels (>850 hPa) the northeasterlies were consistently from the Yellow Sea, passing Shanghai, the biggest city in China. Figure 13a shows a trajectory map, on 20 August as an example from those days. The skies were mostly clear on those days. The concentrations of SO_2 were high (~20 ppbv) at midnight, decreased after sunrise, reached minima (~2 ppbv) in the afternoon, and increased after sunset (Fig. 3 top). These distinct diurnal variations were observed because SO_2 concentrations were high and solar radiation was strong, as photochemical oxidation could rapidly convert SO_2 gas to sulfate particles. The estimated decreasing rate of SO_2 concentration after sunrise was as high as 10% per hour. However, the realistic rate of conversion from SO_2 gas to sulfate particles could be much less, because the planetary boundary layer (PBL) heights are generally greater in the day than at night. The greater space below the PBL and more vigorous mixing caused by heat flux in daytime may also dilute the gas concentrations. Furthermore, Hicks and Wesely (1979)

reported that nocturnal aerodynamic resistances for trace constituents in the air had been measured as greater than those of the daytime. Thus, slower dry deposition for SO_2 should also be observed at night.

Because both SO_2 gas and $SO_4^=$ particles are subjected to the same PBL and aerodynamic conditions the concentration ratios between these two species should cancel such effects. The average of sulfur partition ratios (SPR), which are the mass of S in SO_2 (one half of the SO_2 concentration) divided by S mass in $SO_4^=$ (one third of the $SO_4^=$ concentration) was 3.8 (SD = 2.4) for all night-time samples (n = 24) and 2.2 (SD = 1.5) for all daytime samples (n = 27). The difference was significant at the 95% confidence level. The data suggest that photochemical reactions of SO_2 with atmospheric oxidant OH, NO_x, and O_3, whose concentrations are functions of solar radiation, were important mechanism to produce sulfate aerosols in the daytime.

The end products of SO_2 photo-oxidation are sulfate particles, whose concentrations should be expected to increase in the afternoon and decrease at night. This was indeed observed with the impactor samples collected on 21-23 August and examined with an electron microscope. Figure 14 shows an example of the aerosol size distributions of samples collected on 23 August at various times. More small particles were observed in the afternoon than at night. These excess small particles were identified as containing sulfate, using the EM $BaCl_2$ spot test. Electron microscopy required only a small sample that could be collected in a short period. The good temporal resolution enabled this technique to detect the diurnal variation of sulfate aerosols.

Concentrations of NO_2 showed diurnal variation similar to SO_2, with maxima at night and minima in the afternoon. However, the amplitudes of the variations were weaker, as shown in Fig. 3 (middle). As for O_3 concentrations, the diurnal variation showed that the maxima were in the afternoon (Fig. 3 bottom), just as was expected on these sunny days.

Gases and aerosol concentrations were also strongly influenced by source strengths, which were governed by wind direction and wind speed. Often these diurnal variations, affected by solar radiation, were not observed, especially on days of shifting winds, strong convection, high humidity, or overcast skies. In such cases, other variables would overwhelm the influence of photochemical reactions. For example, on 24-27 August, low-level air trajectories were from the northwest and north (Fig. 13b), and the sky was mostly cloudy. The concentrations diminished to <5 ppbv for SO_2, and <4 ppbv for NO_2. No discernible diurnal variations of their concentrations were observed.

On 28-30 August the 1000 hPa air trajectory changed again to northeasterly, passing Shanghai, but upper air masses were from the north and northwest (Fig. 13c). The surface winds were shifting and the skies were partly cloudy. Although the hourly average SO_2 concentrations were high, fluctuating between 5 and 25 ppbv. and the NO_2 concentrations varied from 4 to 8 ppbv, no discernible diurnal variations for SO_2 and NO_2 were observed on these obscured days.

On 4 September the air trajectories were from the southeast (Fig. 13d).

The SO_2 concentrations decreased to 1-3 ppbv and NO_2 concentrations were 2-4 ppbv (Fig. 4). Again little diurnal variation was observed as the air was relatively clean.

In addition to photo-oxidation, SO_2 can also be adsorbed on atmospheric aerosols such as dust and soot particles, which usually contain mineral elements that can catalytically oxidize SO_2 to sulfate. From electron microscopic spot tests with $BaCl_2$ on impactor samples, we observed 80-99% of small particles ($d < 0.7$ μm) contained sulfate, which was probably produced by photo-oxidation followed by homogeneous nucleation. We also observed that 10-90% larger particles in various samples were also coated with a layer of sulfate, which was most likely formed by catalytic oxidation or heterogeneous nucleation of H_2SO_4. From the $SO_4^=$ mass size distribution (Fig. 10), 60% of the total mass was in particles with $d < 0.43$ μm, most probably formed through homogeneous nucleation; 25% of the mass was in particles with 0.43 $\mu m < d < 1$ μm and the rest with $d > 1$ μm. These larger particles containing $SO_4^=$ had probably formed by heterogeneous nucleation.

Because no measurements of NH_3 gas were conducted, the partition ratios between NH_3 and NH_4^+ are unknown. Because NH_3 is the only atmospheric alkaline gas, it could rapidly react with acidic gases such as H_2SO_4 to form ammonium sulfate particles. The correlation coefficient (r) between the concentrations of NH_4^+ and $SO_4^=$ in 51 samples was 0.81, which was significant at the 95% confidence level. The coefficient of determination ($R = r^2$) was 0.66, suggesting 66% of the mole concentration of $SO_4^=$ could be associated with NH_4^+. Fig. 15 shows the least-squares fit line between the molar concentrations of NH_4^+ and $SO_4^=$, $[NH_4^+] = 0.50 + 0.74[SO_4^=]$. The molar ratio of NH_4^+ and $SO_4^=$ for pure $(NH_4)_2SO_4$ should be 2 and for pure NH_4HSO_4 should be 1. Our data showed the ratio (slope of the line) was 0.74, indicating portions of $SO_4^=$ were associated with other cations.

The r value between molar concentrations of Ca^{++} and $SO_4^=$ was 0.76 ($R = 0.58$), which was also statistically significant. Figure 16 shows the relationship between these two ions, $[Ca^{++}] = 0.05 + 0.31[SO_4^=]$. Since calcite is a common soil component in China, it is very likely that portions of sulfuric acid reacted with Ca^{++} and were neutralized by it to form $CaSO_4$ in aerosols. Indeed, the pH values of the aerosol solutions were generally > 5.7, suggesting that the aerosol particles were not the culprits in acidic precipitation in the region.

The r value between NH_4^+ and NO_3^- was 0.57 ($R = 0.32$), which suggests a weak association between NO_3^- and NH_4^+ in aerosols. Fig. 17 shows the poor correlation between them. The dissimilarity in size distributions of these two ions (Fig. 10) also indicates that they did not coexist in the majority of the individual particles.

The r value between NO_3^- and $SO_4^=$ was 0.79 ($R = 0.62$), indicating significant correlation. Fig. 17 shows their relationship, $[NO_3^-] = -0.17 + 0.29[SO_4]$. Since both ions were anthropogenic pollutants (SO_2, generated from combustion of fossil fuel, is a precursor for $SO_4^=$, whereas NO, produced by high-temperature fixation of atmospheric oxygen and nitrogen, is a precursor for NO_2 and NO_3^-), they could share common sources and pathways. However, the

ratio of molar concentrations between NO_3^- and $SO_4^=$ (as the slope of the line) was 0.29, meaning NO_3^- concentrations were much lower than $SO_4^=$ concentrations in the aerosols.

During the sampling period, two major rain events occurred that might have affected air chemistry at the station. Late September typhoon #9120 traveled northward in the East China Sea (Fig. 19). Although the eye of the typhoon did not land on shore, on 24-26 September intermittent rain falling at the station was probably induced by the system. The station accumulated 27 mm of rainwater. The surface air trajectories remained constantly from the northeast before, during, and after this rain event. However, 850 and 700 hPa winds shifted from northerly to southeasterly during these days. Another rain event occurred on 2-4 October. At that time typhoon # 9121 moved from the South China Sea toward the East China Sea. However, the air trajectories arriving at the station during this period were from west at 500 hPa and from north at levels >850 hPa. The rain event, which yielded 23 mm of rainwater at the station, did not appear to be associated with the co-occurrent typhoon. Table 3 shows the concentrations of elements in two sets of samples; in each set, one sample was collected before and another was collected after a major rain event. The data showed all species had greater concentrations before the rain than after. This demonstrated that wet deposition is an effective mechanism for cleaning the air. The concentration ratios of before and after a rain event varied from species to species, and from event to event. suggesting the rate of washout varied with individual species. Perhaps water affinities of individual species, size distribution of the particles, and raindrop size distribution, all influence the scavenging efficiencies. Aerosol samples collected 12 hours after rain events had elemental and ionic concentrations similar to those before the rain. It appears that the washout effect by rain was rather short-lived.

5. SUMMARY AND CONCLUSION

The results of measurements of atmospheric gases and aerosols at Lin-an station are documented in this report. The average concentrations of each species may represent general air chemistry during the sampling period from August to October 1991. However, the data sets should not be considered as statistically representative of long-term means. More interseasonal and interannual measurements are needed to achieve that purpose.

The median SO_2 hourly concentration was 5 ppbv; the minimum was < 0.1 ppbv and the maximum was 35 ppbv. The median hourly concentration of black carbon was 2 $\mu g\ m^{-3}$; the minimum was 0.2 $\mu g\ m^{-3}$ and the maximum was 4.6 $\mu g\ m^{-3}$. The vast temporal variabilities of each parameter were analyzed and interpreted in relation to meteorological variables. Generally wind directions and wind speeds are dominant factors. When air masses arrived from Shanghai with the northeasterlies at a steady speed of 2-4 $m\ s^{-1}$, concentrations of SO_2, NO_2, and black carbon were usually above the average. Occasionally, high concentrations were also observed when winds were from southwest where the city of Lin-an is located. Lower concentrations were found when the southeasterlies delivered clean air from the sea, or when the northwesterlies transported air masses from the mountains.

Diurnal variations of SO_2 concentrations were observed only on sunny days under the prevailing northeasterlies, whereas photochemical oxidation followed by homogeneous nucleation could rapidly convert SO_2 gas to $SO_4^=$ particles. Although no significant differences in aerosol $SO_4^=$ concentrations were found between day (14.57 μgm^{-3}) and night (15.70 μgm^{-3}), the average sulfur mass partition ratios between SO_2 and $SO_4^=$ were computed to be 3.2 for nighttime and 2.1 for daytime, and the difference was statistically significant. The data indicate that more SO_2 was converted to $SO_4^=$ particles in the day than at night.

Aerosol $SO_4^=$ and NH_4^+ had a similar size distribution with > 60% of mass present in particles $d < 0.43$ μm. Good correlation was found between the concentrations of these two ions ($r = 0.81$), suggesting that most of these small particles were NH_4SO_4 or NH_4HSO_4. More than 90% of Ca^{++} mass and 40% of $SO_4^=$ mass were present in particles with $d > 0.65$ μm. And good correlation was also found between the concentrations of Ca^{++} and $SO_4^=$ ($r = 0.76$), suggesting that $CaSO_4$ probably was present in larger particles.

The average NO_3^- concentration was less than one third of $SO_4^=$ by mole and less than about one-fifth by mass. Good correlation was found between these two ions ($r = 0.79$), indicating their common sources. Unlike for sulfate particles, which were mostly small, for NO_3^- more than 90% of the mass was present in particles $d > 1$ μm. This suggests that NO_3^- was probably nucleated and titrated by existing aerosol particles.

The average total particle mass was 242.1 $\mu g\ m^{-3}$, and average crustal dust concentration was 56.3 $\mu g\ m^{-3}$, indicating that both natural dust and anthropogenic aerosols had high concentrations over Lin-an station. After heavy rain events the concentrations of both soil elements and enriched species reduced to almost half of the pre-event values. Wet deposition, in addition to dry deposition, could be an effective process to remove the air contaminants. Furthermore, vertical convection and horizontal advection by the westerlies or jet streams were also effective processes for removing air pollution from the station. The measured data provide a useful inventory of source strengths of the trace species that could be transported from China to the West Pacific Ocean. The knowledge of the journey of individual species is very important to climatic change research.

6. ACKNOWLEDGMENTS

We are grateful to Shaw C. Liu, Aeronomy Laboratory, and NOAA Mission Scientist to the PEM-west program, for cooperation and financial support. Thanks are due to Xiuji Zhou, Director of the Chinese Academy of Meteorological Sciences, and Bruce Hicks, Director of NOAA Air Resources Laboratory, for their encouragement and guidance on this project.

7. REFERENCES

Bigg, E.K., Ono, A, and Williams, J.K., 1974. Chemical test for individual submicron aerosol particles. Atmos. Environ., 8, 1-13.

Hansen, A.D.K., and T. Novakov, 1988. Aerosol black carbon measurements over the Western Atlantic Ocean. Global Biogeochem. Cycles, 2, 41-45.

Harris, J., 1982. The GMCC atmospheric trajectory program. NOAA Tech Memo ERL-ARL-116, NOAA/ERL, Air Resources Laboratory, Boulder, Colorado.

Hicks, B.B., and M.L. Wesely, 1979. Turbulent transfer processes to a surface and interaction with vegetation. In Atmospheric Sulfur Deposition, D.S. Shiner, C.R. Richmond, and S.E. Lindberg (eds.). Ann Arbor Science, Ann Arbor, Michigan, 119-207.

Kopcewicz, B., C. Nagamoto, F. Parungo, J. Miller, H. Sievering, and J. Rosinski, 1991. Morphological studies of sulfate and nitrate particles on the east coast of North America and over the North Atlantic Ocean. Atmos. Res., 26, 245-271.

Liu, S.C., 1992. The transport and distribution of Ozone and precursors during PEM-West/APARE experiment. EOS 73 432A-1.

Luria, M., J.F. Boatman, J. Harris, J. Ray, T. Straube, J. Chin, R.L. Gunter, G. Herbert, T.M. Gerlach, and C.C. Van Valin, 1992. Atmospheric sulfur dioxide at Mauna Loa, Hawaii. J. Geophy. Res., 97, 6011-6022.

NAPAP, 1987. The National Acid Precipitation Assessment Program III Chapter 5. Acid deposition and its gaseous precursors 116 p.

Parungo, F., C. Nagamoto, J. Rosinski, and P. Haagenson, 1986. A study of marine aerosols over the Pacific Ocean. Atmos. Chem., 4, 199-226.

Taylor, S.R., and S.M. McLennan, 1985. The Continental Crust: Its Composition and Evolution. Blackwell, Oxford, 312 pp.

Wang, W., and Q. Shi, 1991. Analysis of the formation of air pollution and acid rain in China. Proceedings of the 2nd IUPAPPA Regional Conference on Air Pollution, Seoul, Korea. Vol. 2, 49-57. Korean Air Pollution Association, Seoul, Korea.

Zhou, M.Y., S.J. Yang, F. Parungo, J. Harris, 1990. Chemistry of marine aerosols over the Western Pacific Ocean. J. Geophys. Res., 95, 1779-1787.

TABLE 1. Average concentrations (ng m^{-3}) and average enrichment factors at 95% confidence intervals

Element	Concentration	Enrichment Factor	Element	Concentration	Enrichment Factor
Na	(1.5 ± 0.4) E3	1.5 ± 0.2	Zr	(2.1 ± 0.7)E1	(7.5 ± 3.2)E1
Mg	(1.3 ± 0.3) E3	1.8 ± 0.5	Mo	3.08 ± 0.85	(5.8 ± 1.2)E1
Al	(4.5 ± 0.6) E3	1.5 ± 0.1	Ag	0.53 ± 0.09	(2.5 ± 0.5)E2
Si	(8.1 ± 1.3) E3	0.8 ± 0.1	In	0.24 ± 0.04	(8.2 ± 2.3)E1
S	(1.1 ± 0.2) E4	(1.5 ± 0.4)E3	Sb	2.84 ± 0.62	(4.2 ± 0.8)E2
Cl	(6.9 ± 3.1) E2	(1.4 ± 0.5)E2	I	(1.3 ± 0.3)E1	(7.7 ± 1.8)E2
K	(2.8 ± 0.9) E3	3.7 ± 1.6	Cs	1.58 ± 0.27	(1.6 ± 0.3)E1
Ca	(7.0 ± 1.2) E3	5.2 ± 0.5	Ba	(4.9 ± 0.9)E1	3.2 ± 0.3
Sc	0.6 ± 0.1	0.7 ± 0.0	La	2.54 ± 0.38	2.3 ± 0.1
Ti	(2.4 ± 0.5) E2	1.3 ± 0.2	Ce	4.77 ± 0.68	2.2 ± 0.1
V	5.0 ± 0.9	1.2 ± 0.1	Nd	1.15 ± 0.48	0.9 ± 0.3
Cr	9.6 ± 2.1	(2.8 ± 0.5)E2	Sm	0.38 ± 0.06	1.6 ± 0.1
Mn	(6.9 ± 1.1) E1	1.9 ± 0.2	Eu	0.12 ± 0.01	3.7 ± 0.8
Fe	(2.0 ± 0.3) E3	1.0 ± 0.0	Tb	0.07 ± 0.02	2.2 ± 0.8
Co	1.0 ± 0.2	1.5 ± 0.7	Yb	0.13 ± 0.03	1.1 ± 0.2
Ni	3.1 ± 2.3	1.5 ± 1.3	Lu	0.03 ± 0.01	1.7 ± 0.2
Cu	(1.4 ± 0.7) E1	7.8 ± 3.8	Hf	0.32 ± 0.05	2.8 ± 0.3
Zn	(1.6 ± 0.3) E2	(7.2 ± 1.3)E1	Ta	0.07 ± 0.02	1.0 ± 0.7
Ga	(1.1 ± 0.6) E1	(3.5 ± 2.9)E2	W	0.89 ± 0.18	(1.6 ± 0.3)E1
As	0.7 ± 0.1	(1.0 ± 0.1)E1	Au	0.01 ± 0.00	(7.7 ± 1.2)E1
Se	3.8 ± 0.6	(2.4 ± 0.4)E2	Pb	(2.6 ± 0.4)E2	(4.5 ± 0.8)E4
Br	(1.7 ± 0.7) E1	(1.8 ± 0.3)E2	Th	0.87 ± 0.14	2.3 ± 0.1
Rb	(1.3 ± 0.2) E1	5.1 ± 1.6	U	0.33 ± 0.05	3.4 ± 0.3

En = 10^n

TABLE 2. Average concentrations ($\mu g\ m^{-3}$) and 95% confidence intervals for the ions in water-soluble aerosols

Ion	Concentration
$SO_4^=$	15.1 ± 2.0
NO_3^-	1.8 ± 0.6
Cl^-	0.6 ± 0.4
Na^+	1.7 ± 0.6
K^+	2.0 ± 0.6
NH_4^+	3.0 ± 0.4
Ca^{++}	2.2 ± 0.5
Mg^{++}	0.2 ± 0.1

TABLE 3. Concentrations ($\mu g\ m^{-3}$) of the species in the aerosol samples collected before and after the two major rain events

Species	Concentration		Ratio	Concentration		Ratio
	Before 9/23	After 9/27		Before 10/12	After 10/14	
Si	8.2	2.8	2.9	5.6	2.1	2.7
Al	4.0	2.2	1.8	4.1	1.6	2.6
Fe	1.7	1.2	1.4	1.4	0.5	2.8
Sc	5.6 E-4	2.7 E-4	2.0	4.7 E-4	1.7 E-4	2.8
As	7.1 E-4	1.9 E-4	3.7	3.5 E-4	1.0 E-4	3.5
S	1.5 E1	6.3	2.4	1.5 E1	9.2	1.7
Sb	3.4 E-3	1.5 E-3	2.3	1.5 E-3	7.8 E-4	3.2
Se	3.0 E-3	2.6 E-3	1.2	4.5 E-3	1.4 E-3	3.2
Na	1.8	0.7	2.4	1.8	0.43	4.1
Cl	0.34	0.14	2.4	0.43	0.12	3.7
C	2.3	1.1	2.1	--	--	--
$SO_4^=$	1.5 E1	1.1 E1	1.4	1.8 E1	1.0 E1	1.8
NO_3^-	3.0	0.25	1.2 E1	0.93	0.63	1.5
NH_4^+	4.3	2.5	1.7	3.2	3.2	1.0

En = 10^n

Fig. 1. Map of the region and photographs of Lin-an station.

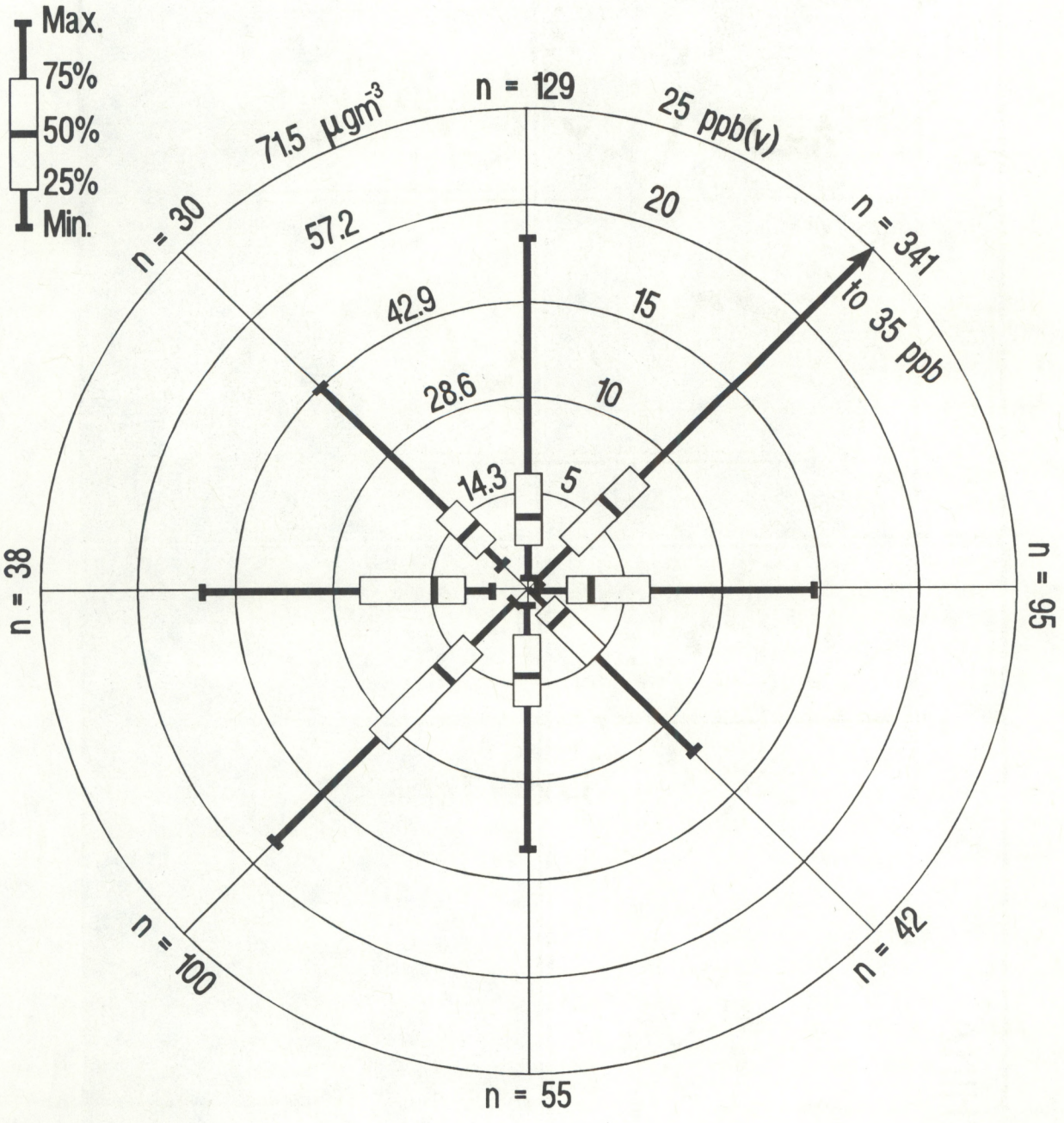

Fig. 2. SO_2 rose showing concentrations of SO_2 in eight wind sectors; n is the number of hours that measurements were taken in that direction.

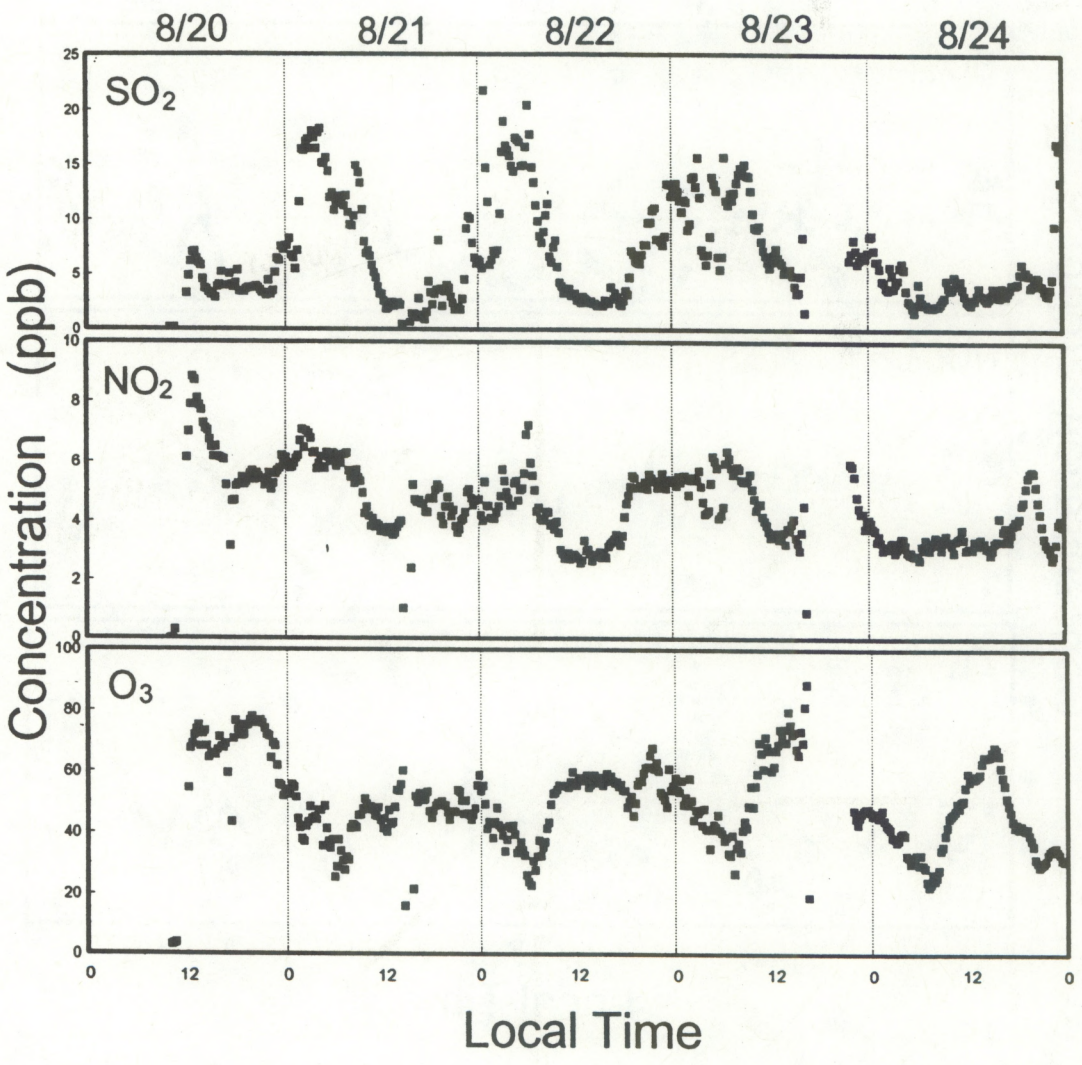

Fig. 3. Concentrations of SO_2 (top), NO_2 (middle), and O_3 (bottom) measured on 20-24 August 1991.

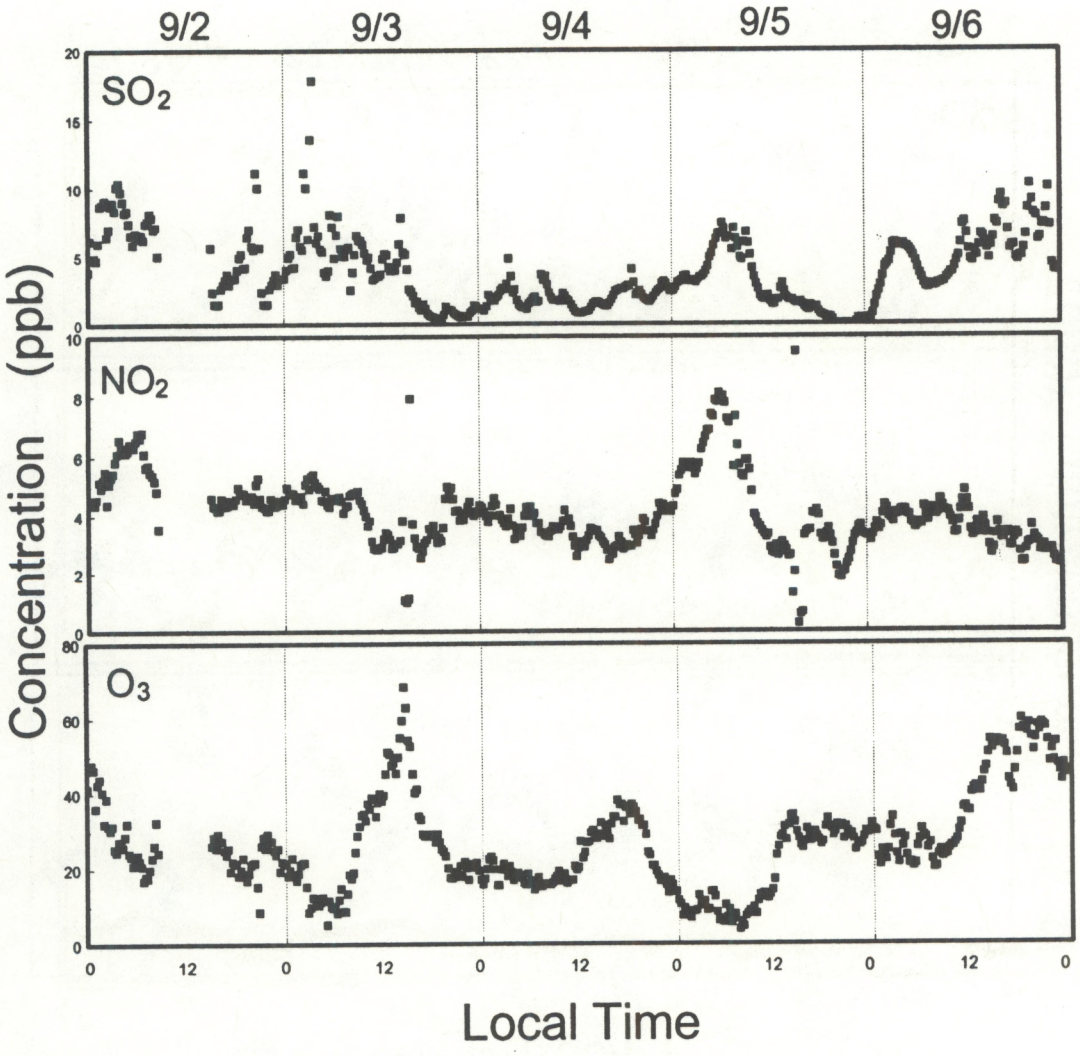

Fig. 4. Same as Fig. 3, but on 2-6 September.

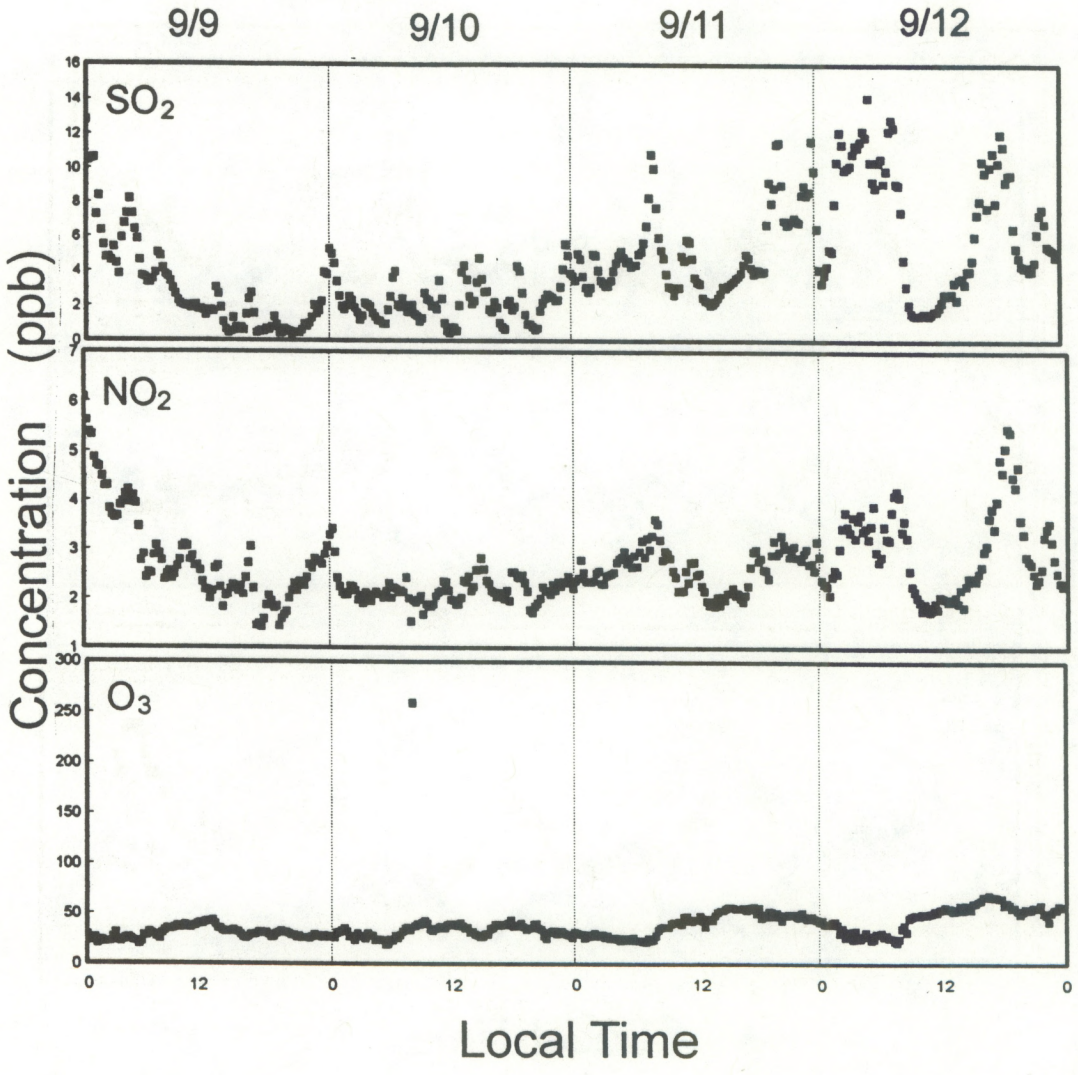

Fig. 5. Same as Fig. 3, but on 9-12 September.

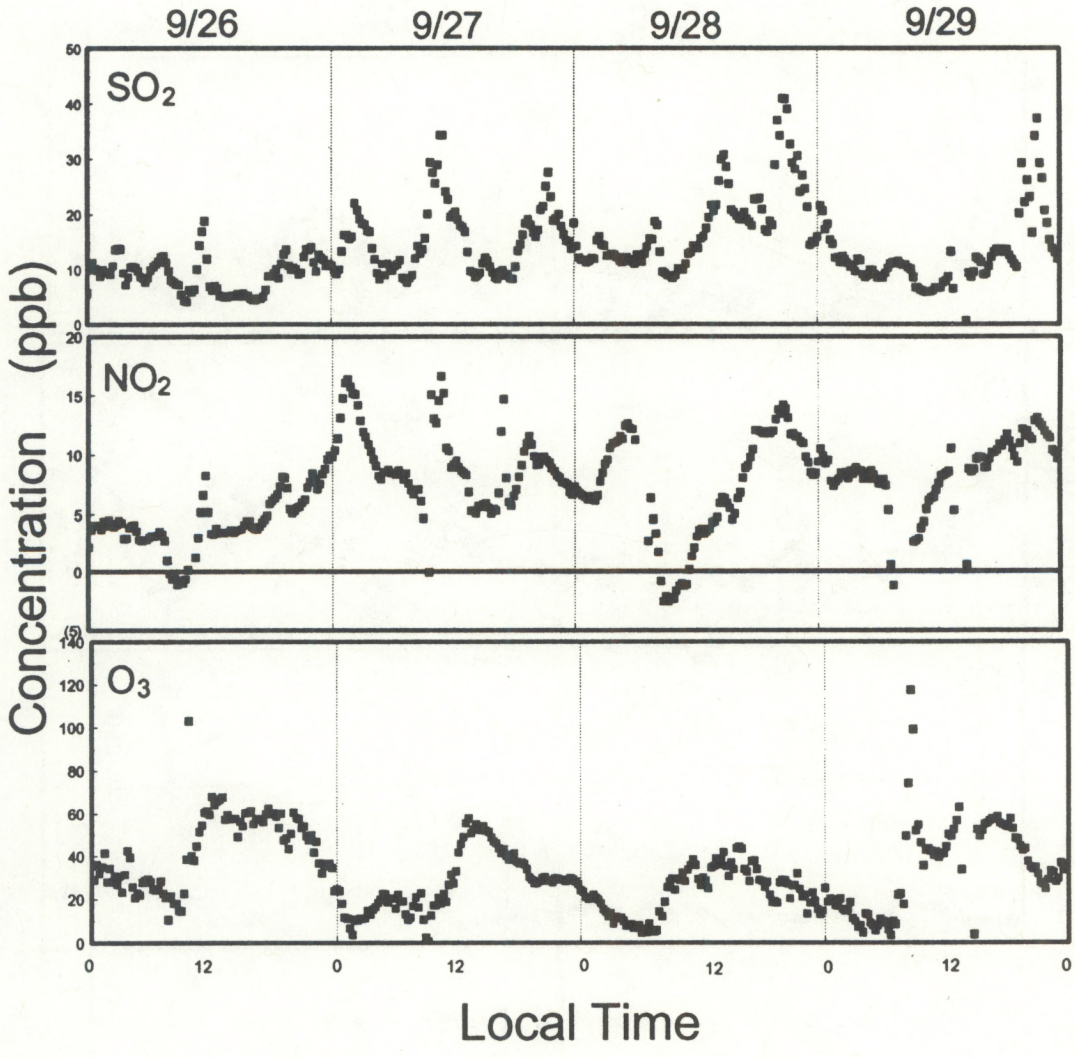

Fig. 6. Same as Fig. 3, but on 26-29 September.

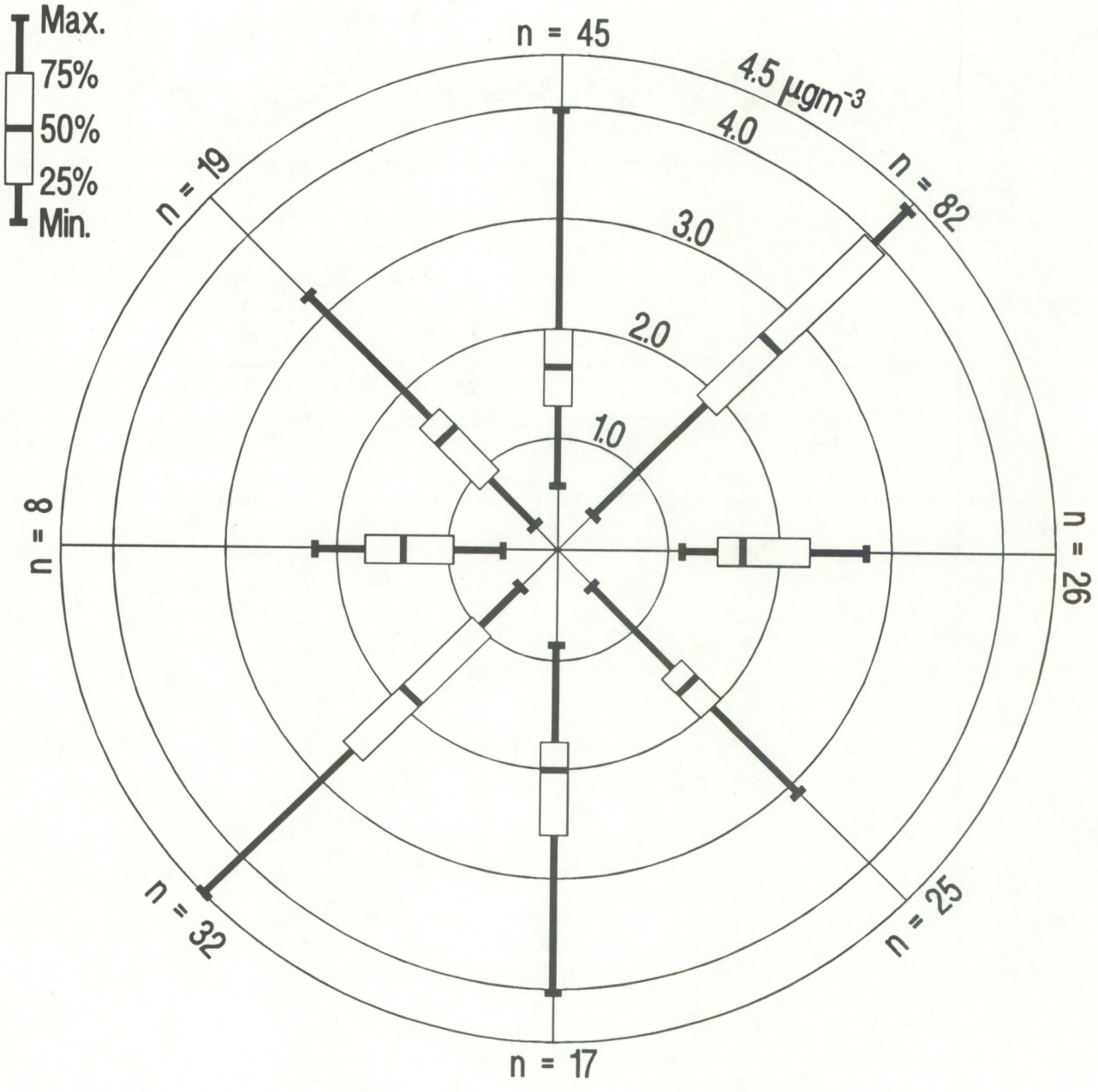

Fig. 7. Black carbon rose shows concentrations of black carbon in eight wind sectors; n is number of hours measurements were taken in that direction.

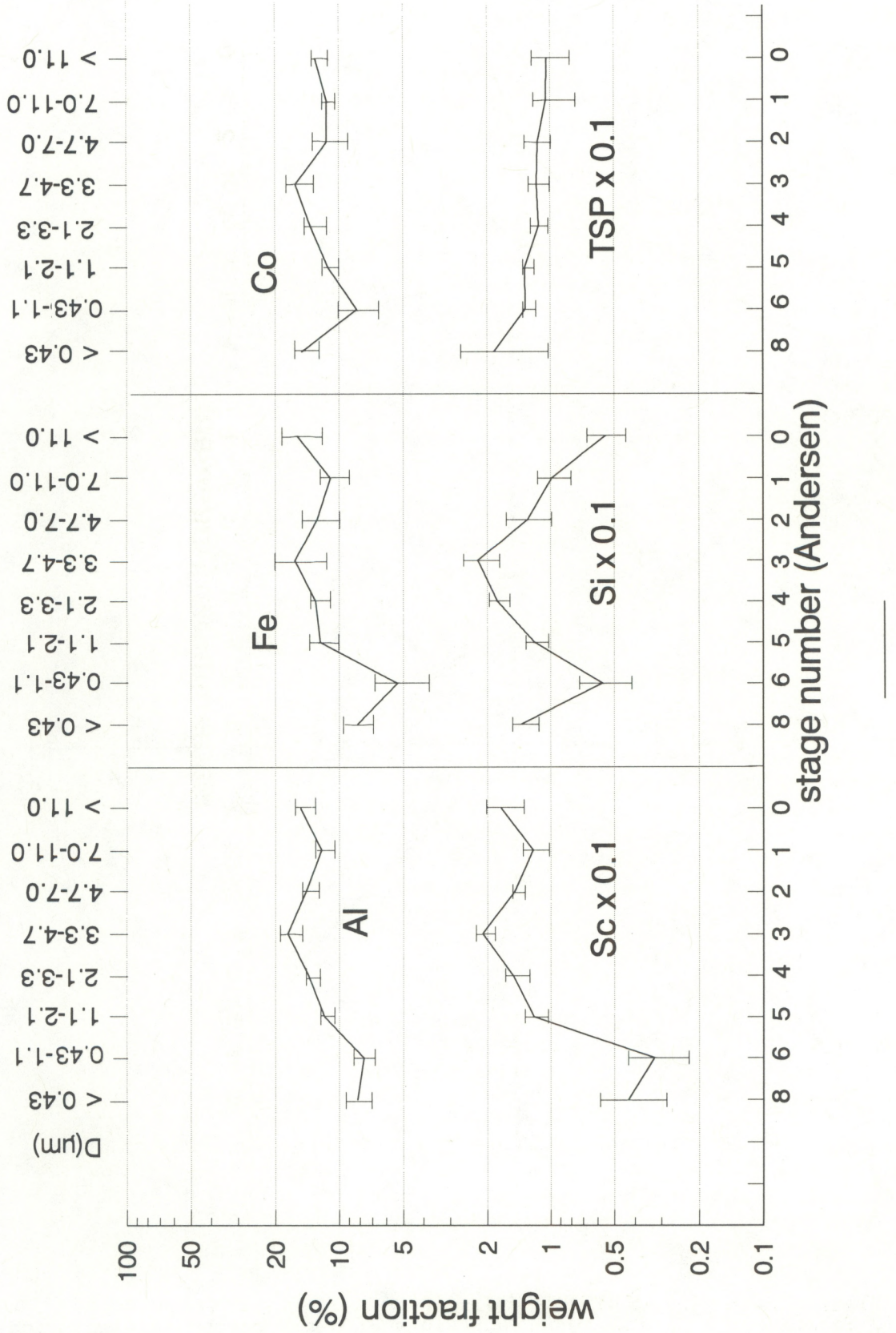

Fig. 8. Size distributions of Al, Fe, Co, Sc, Si, and total suspended particles (TSP). The bars show 95% confidence intervals, and the data points are averages of weight fractions for individual stages.

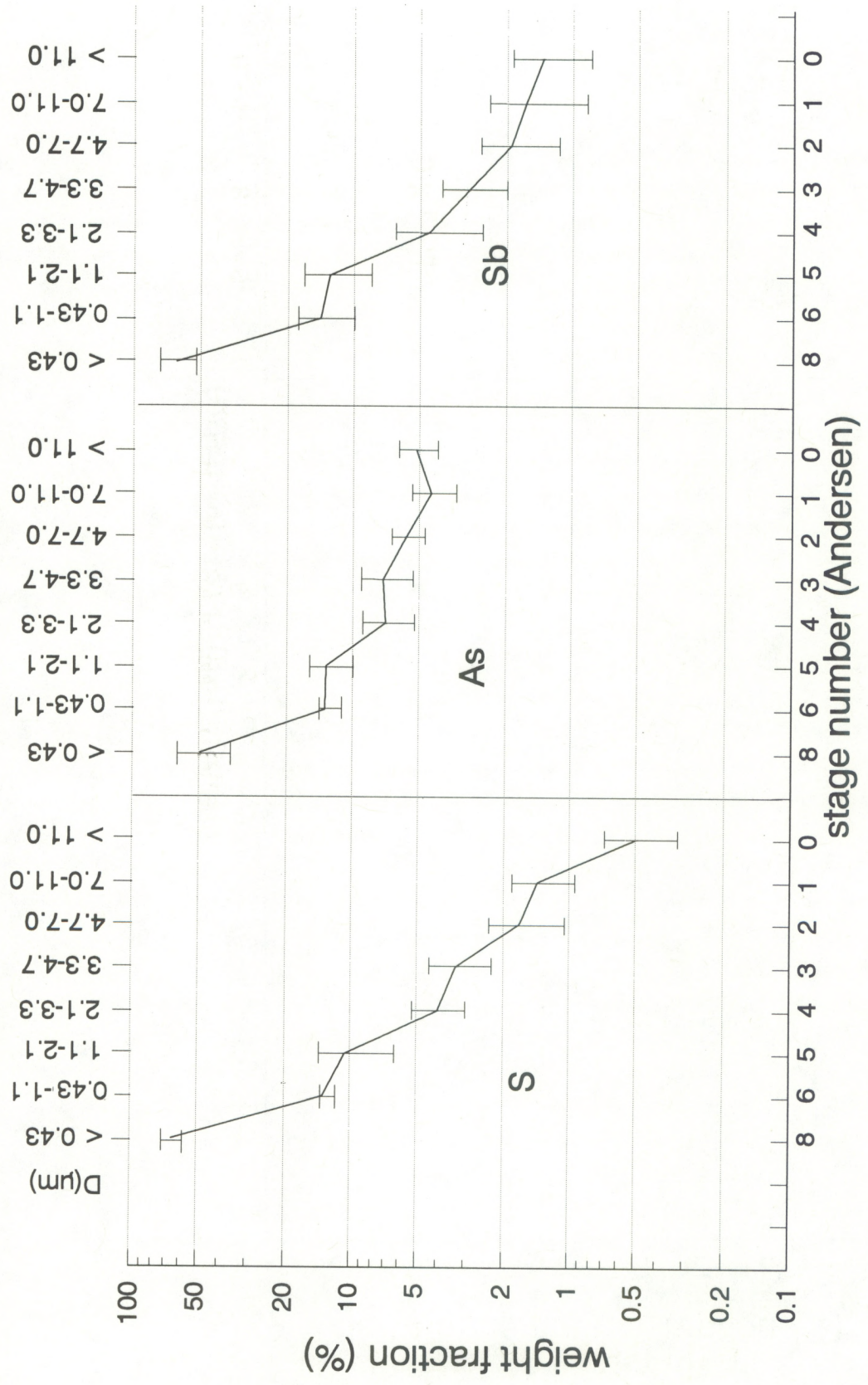

Fig. 9. Size distributions of S, As, and Sb, as in Fig. 8.

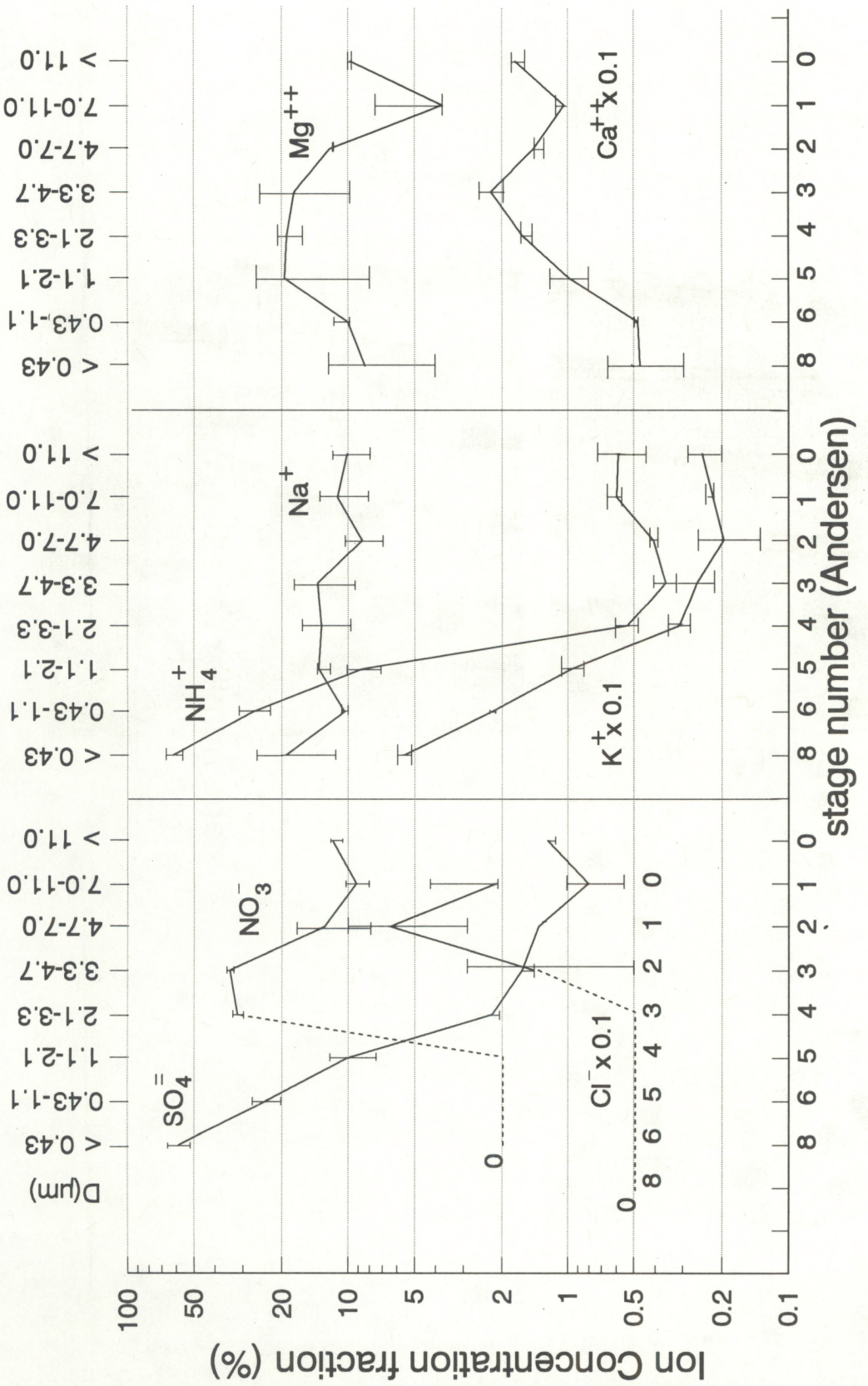

Fig. 10. Size distribution of $SO_4^=$, NO_3^-, Cl^-, NH_4^+, Na^+, K^+, Mg^{++}, and Ca^{++}. as in Fig. 8.

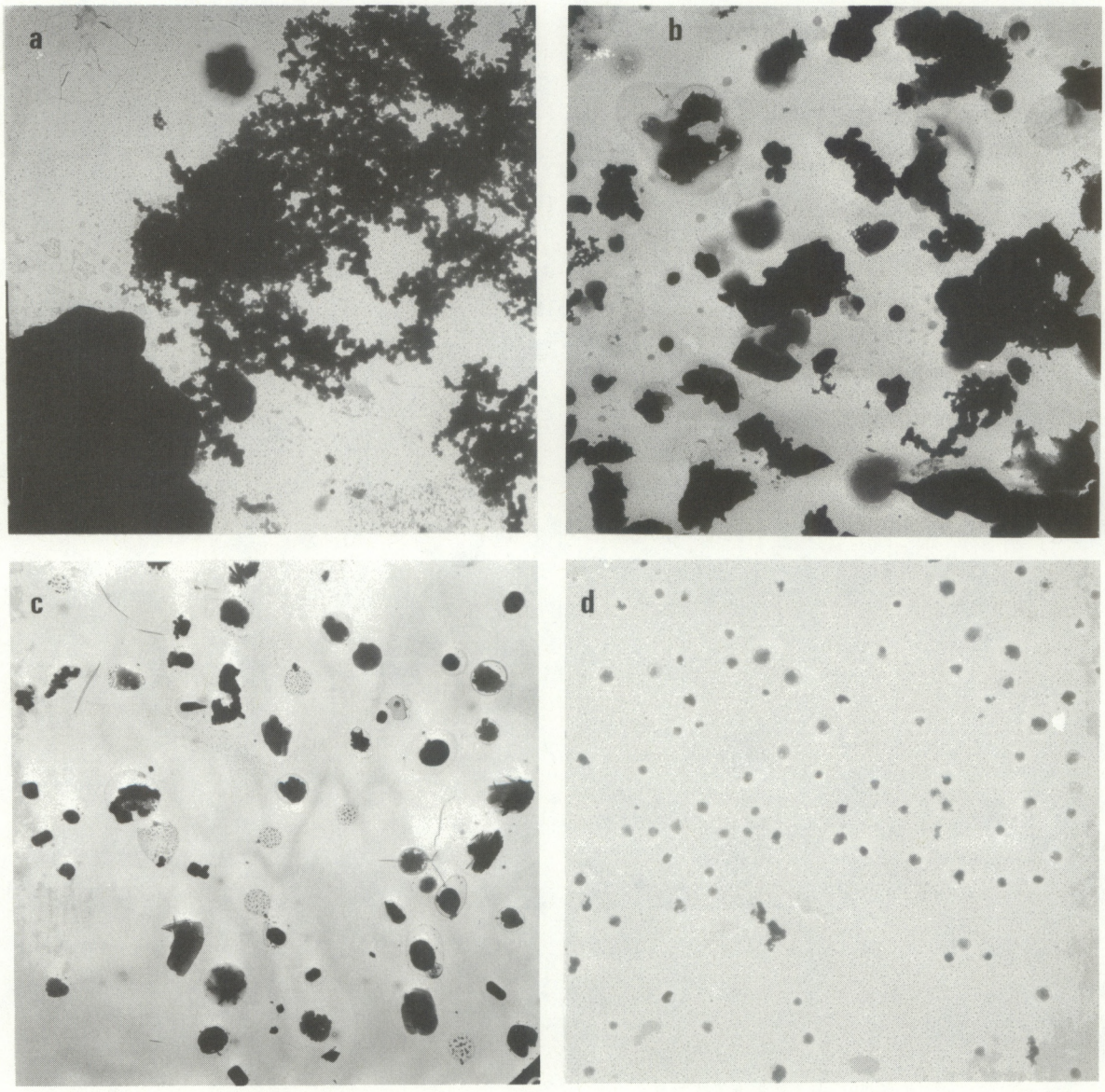

Fig. 11. Morphology of aerosol particles collected on four stages of a cascade impactor at Lin-an Station: (a) Stage 1 ($d > 5\ \mu m$), (b) Stage 2 ($d > 2\ \mu m$), Stage 3 ($d > 0.7\ \mu m$), (d) Stage 4 ($d < 0.7\ \mu m$).

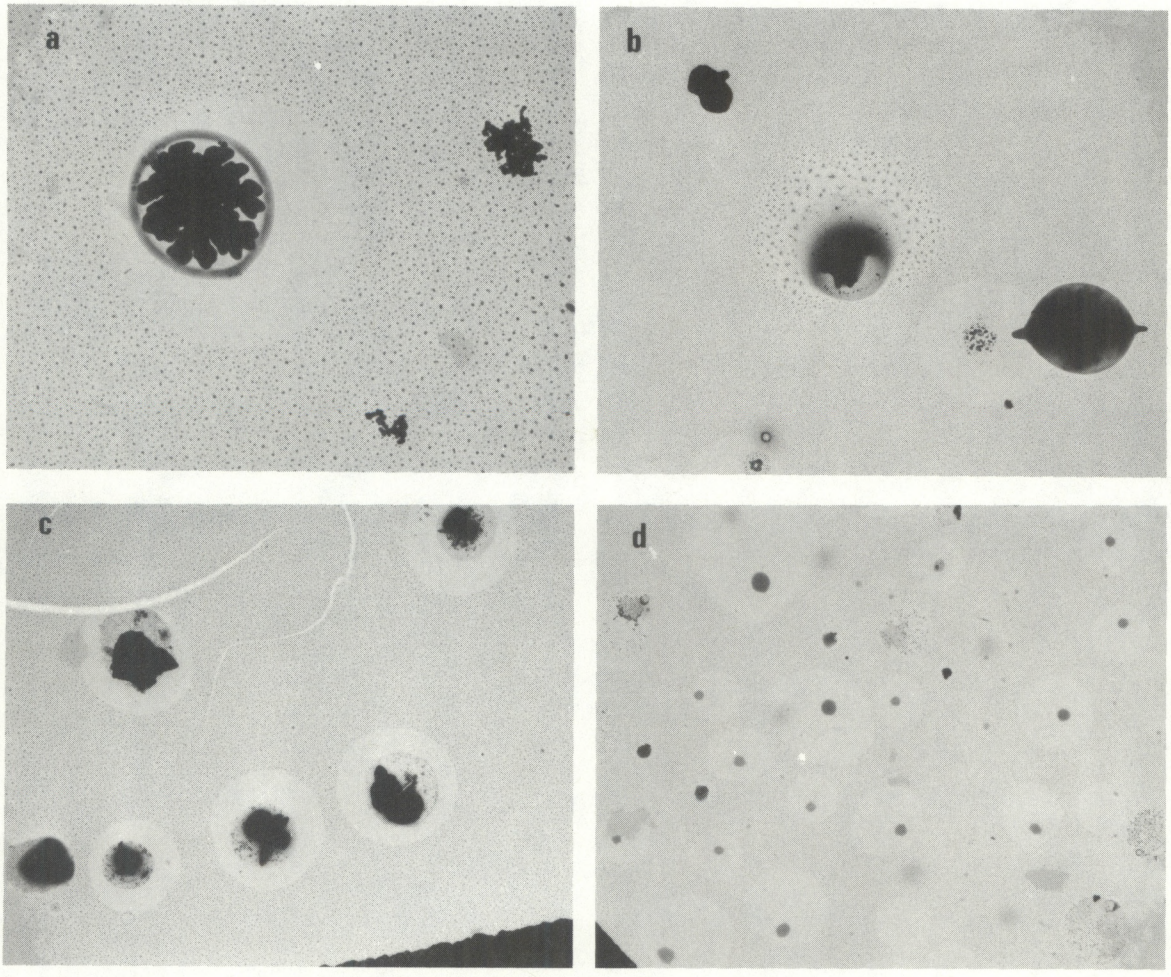

Fig. 12. Electron micrographs of aerosol particles treated with $BaCl_2$. The hollow ring surrounding a particle indicates its $SO_4^=$ content: (a) Stage 1, (b) Stage 2, (c) Stage 3, (d) Stage 4.

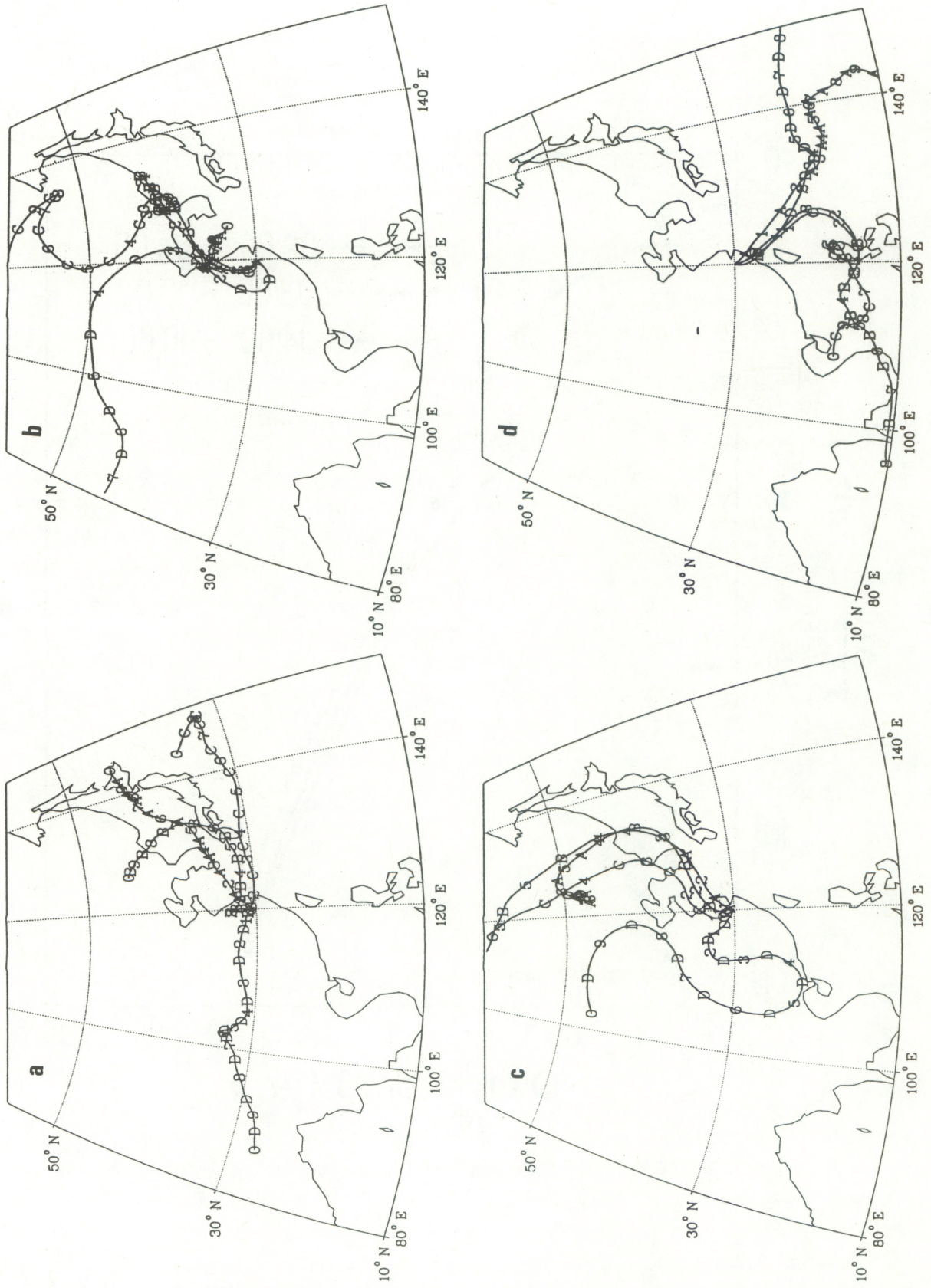

Fig. 13. Ten-day backward air trajectories arriving at Lin-an on (a) 20 August 1991 at 0000 UT, (b) 24 August at 0000 UT, (c) 29 August at 1200 UT, and (d) 5 September at 0000 UT. A, 1000 hPa; B, 850 hPa; C, 700 hPa; D, 500 hPa.

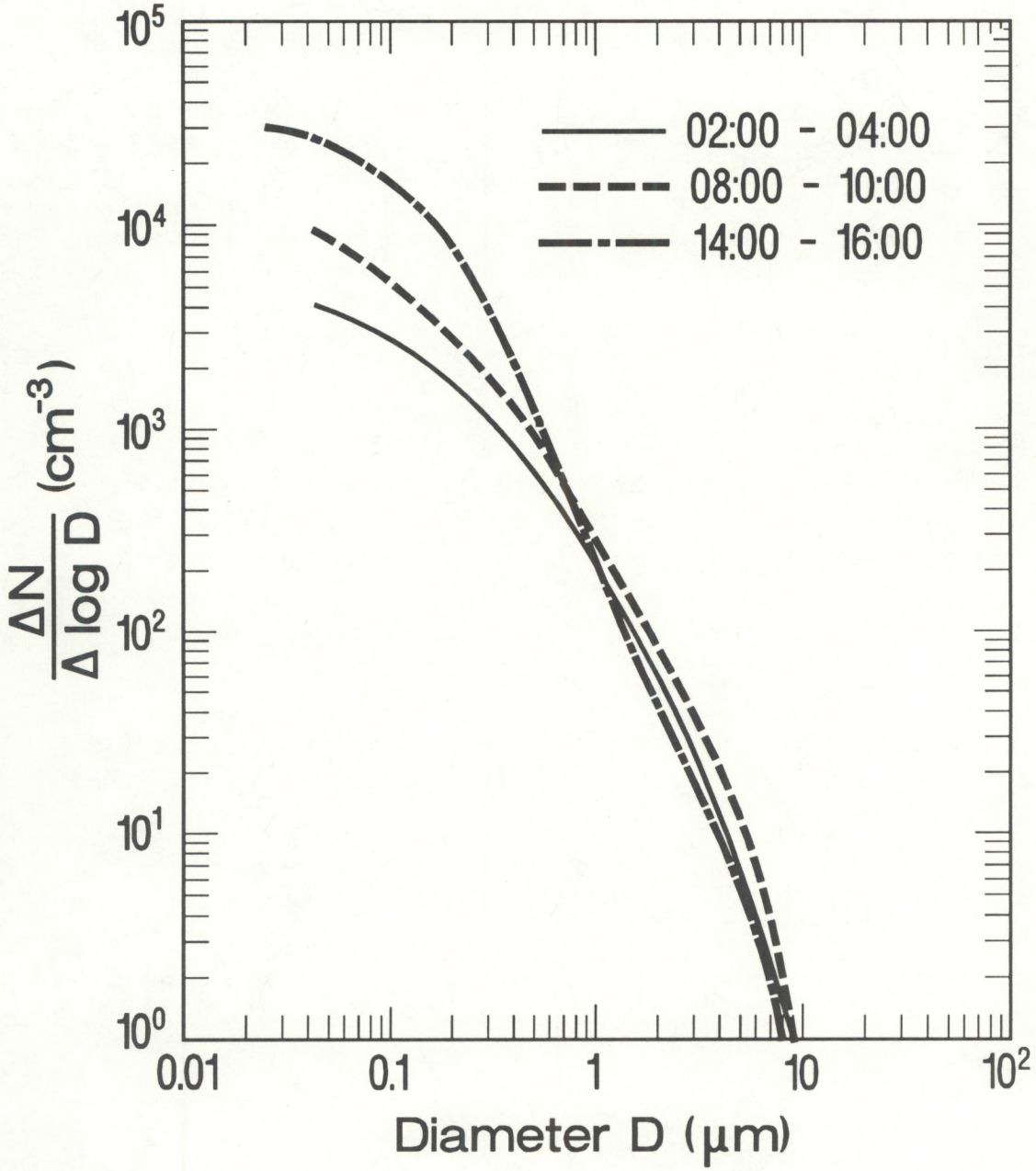

Fig. 14. Particle number size distributions of the samples collected at different times on 23 August 1991.

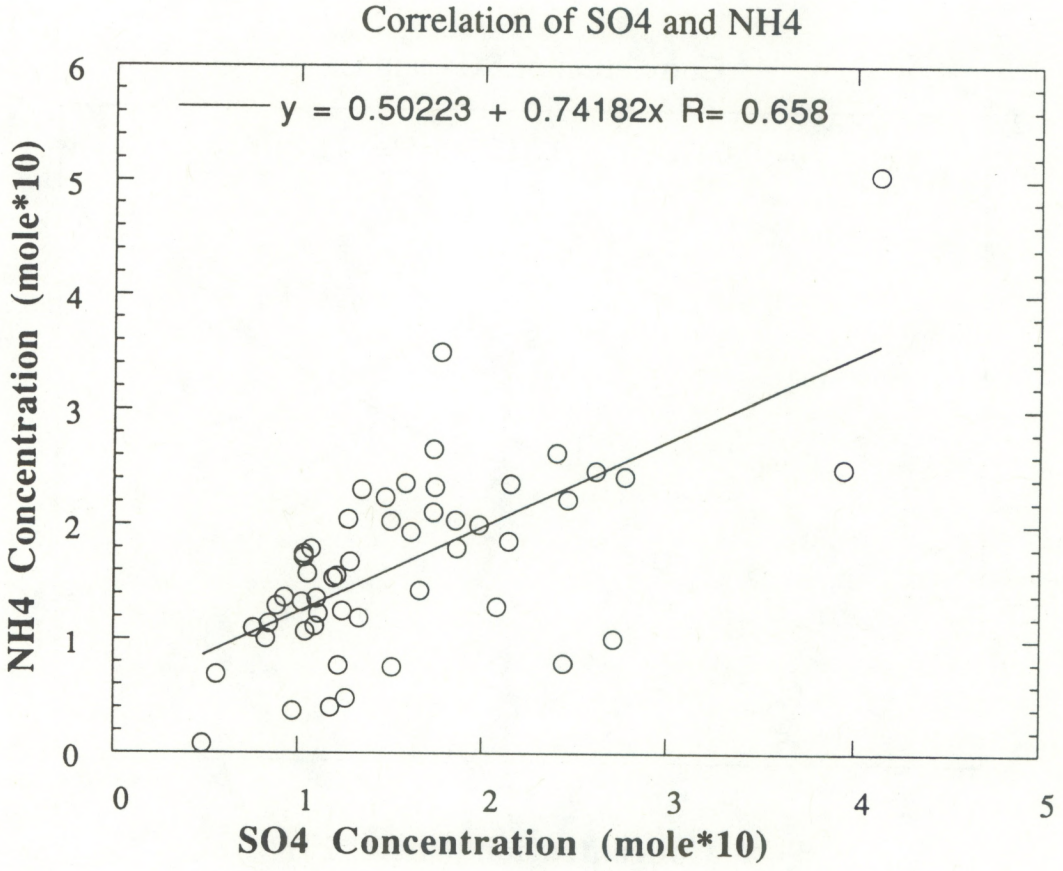

Fig. 15. Correlation of molar concentration between NH_4^+ and $SO_4^=$.

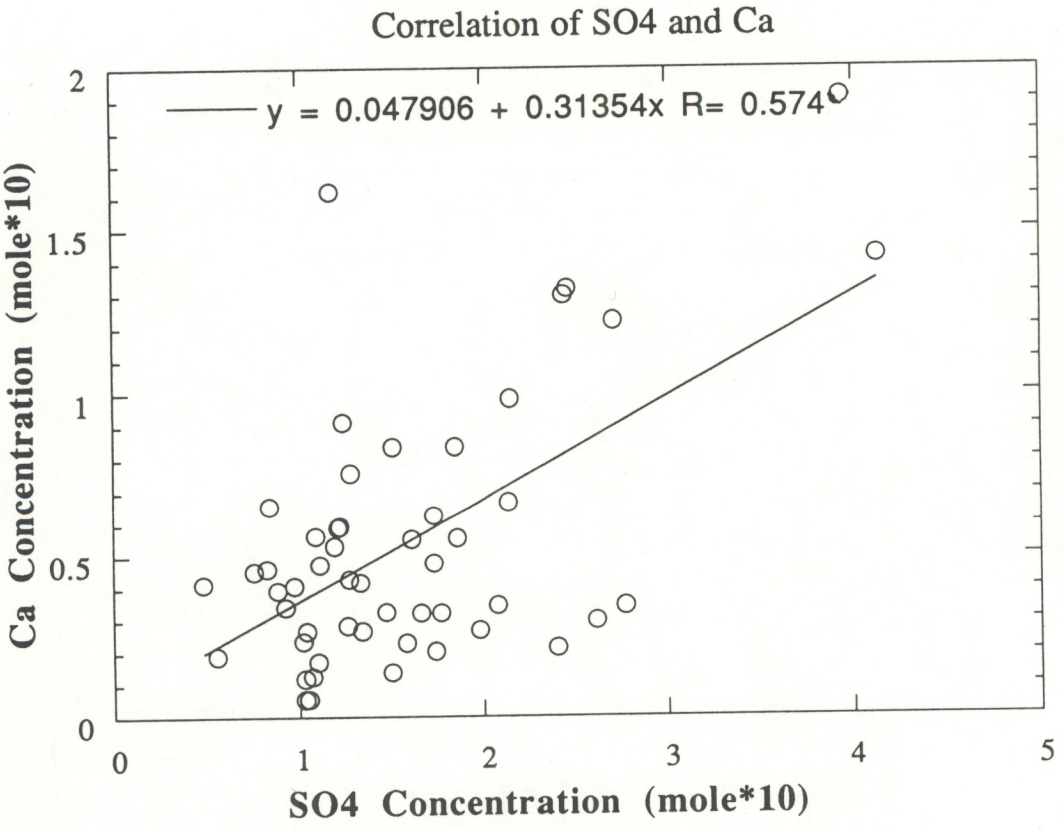

Fig. 16. Correlation of molar concentration of Ca^{++} and $SO_4^{=}$.

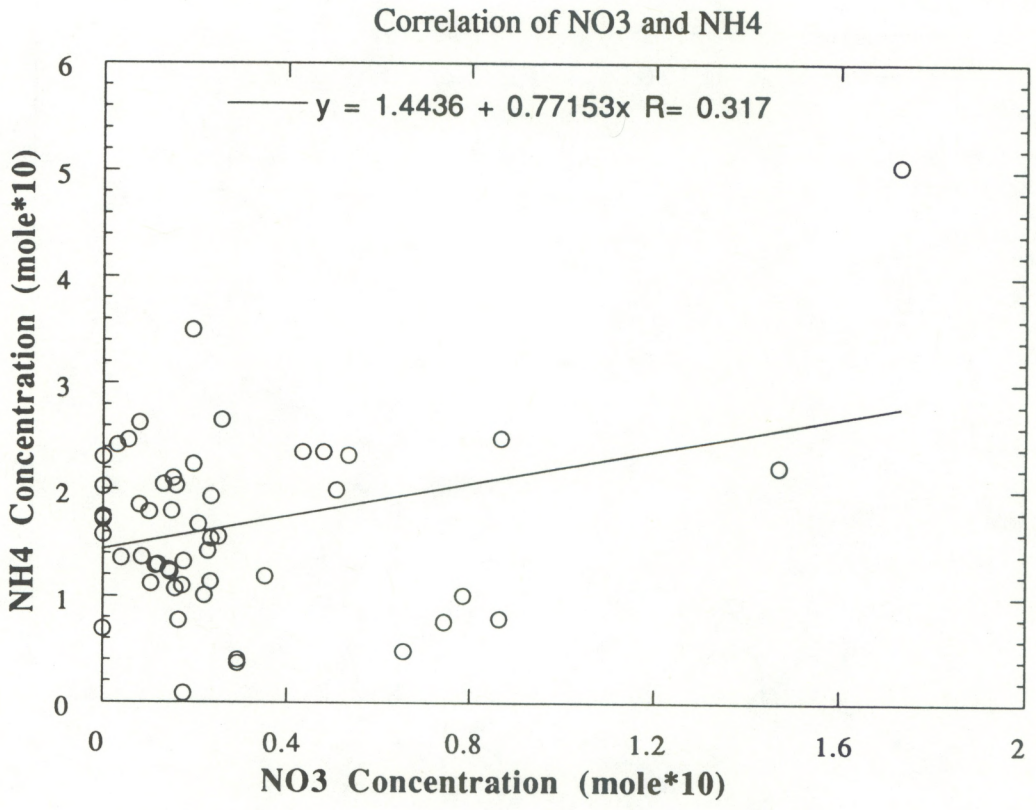

Fig. 17. Correlation of molar concentration of NH_4^+ and NO_3^-.

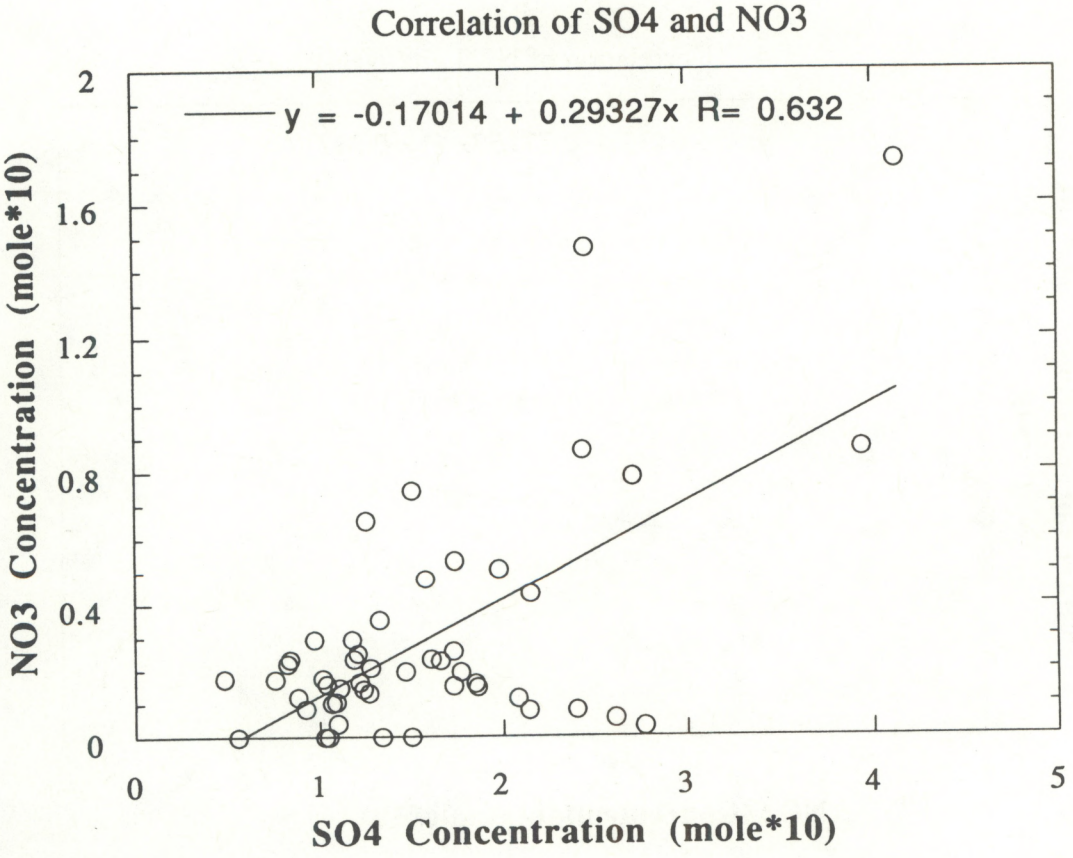

Fig. 18. Correlation of molar concentration of NO_3^- and $SO_4^=$.

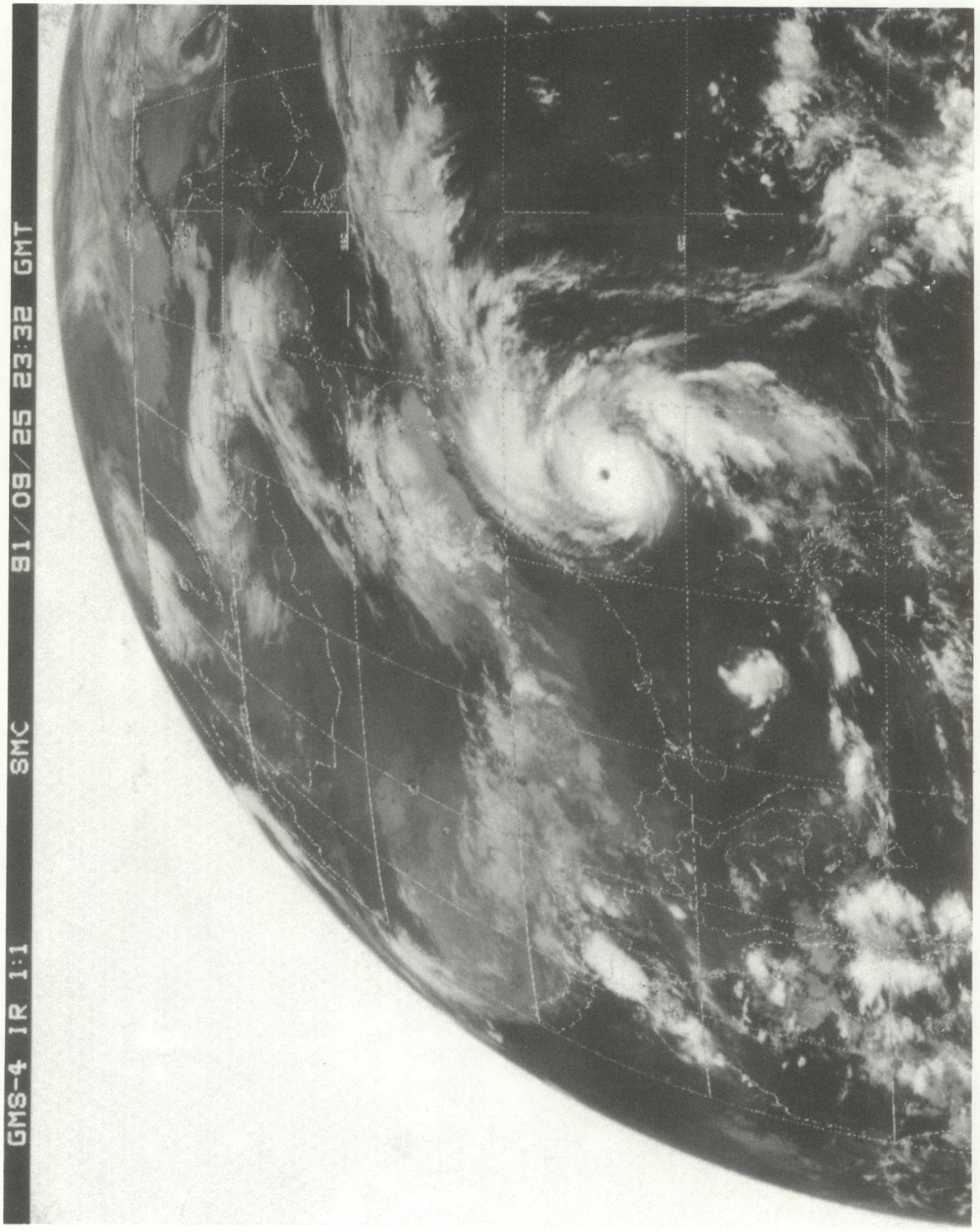

Fig. 19. Satellite image of typhoon #9120 taken on 25 September 1991 at 2332 GMT.

*U.S. GOVERNMENT PRINTING OFFICE: 1993-774-025/89006